

## Frictional slip of granite at hydrothermal conditions

Michael L. Blanpied, David A. Lockner, and James D. Byerlee

U. S. Geological Survey, Menlo Park, California

**Abstract.** Sliding on faults in much of the continental crust likely occurs at hydrothermal conditions, i.e., at elevated temperature and elevated pressure of aqueous pore fluids, yet there have been few relevant laboratory studies. To measure the strength, sliding behavior, and friction constitutive properties of faults at hydrothermal conditions, we slid laboratory granite faults containing a layer of granite powder (simulated gouge). Velocity stepping experiments were performed at temperatures of 23° to 600°C, pore fluid pressures  $P_{H_2O}$  of 0 (“dry”) and 100 MPa (“wet”), effective normal stress of 400 MPa, and sliding velocities  $\dot{V}$  of 0.01 to 1  $\mu\text{m/s}$  (0.32 to 32 m/yr). Conditions were similar to those in earlier tests on dry granite to 845°C by Lockner et al. (1986). The mechanical results define two regimes. The first regime includes dry granite up to at least 845° and wet granite below 250°C. In this regime the coefficient of friction is high ( $\mu = 0.7$  to 0.8) and depends only modestly on temperature, slip rate, and  $P_{H_2O}$ . The second regime includes wet granite above ~350°C. In this regime friction decreases considerably with increasing temperature (temperature weakening) and with decreasing slip rate (velocity strengthening). These regimes correspond well to those identified in sliding tests on ultrafine quartz. We infer that one or more fluid-assisted deformation mechanisms are activated in the second, hydrothermal, regime and operate concurrently with cataclastic flow. Slip in the first (cool and/or dry) regime is characterized by pervasive shearing and particle size reduction. Slip in the second (hot and wet) regime is localized primarily onto narrow shear bands adjacent to the gouge–rock interfaces. Weakness of these boundary shears may result either from an abundance of phyllosilicates preferentially aligned for easy dislocation glide, or from a dependence of strength on gouge particle size. Major features of the granite data set can be fit reasonably well by a rate- and temperature-dependent, three-regime friction constitutive model (Chester, this issue). We extrapolate the experimental data and model fit in order to estimate steady state shear strength versus depth along natural, slipping faults for sliding rates as low as 31 mm/yr. We do this for two end-member cases. In the first case, pore pressure is assumed hydrostatic at all depths. Shallow crustal strength in this case is similar to that calculated in previous work from room temperature friction data, while at depths below about 9–13 km (depending on slip rate), strength becomes less sensitive to depth but sensitive to slip rate. In the second case, pore pressure is assumed to be near-lithostatic at depths below ~5 km. Strength is low at all depths in this case (<20 MPa, in agreement with observations of “weak” faults such as the San Andreas). The predicted depth of transition from velocity weakening to velocity strengthening lies at about 13 km depth for a slip rate of 31 mm/yr, in rough agreement with the seismic-aseismic transition depth observed on mature continental faults. These results highlight the importance of fluid-assisted deformation processes active in faults at depth and the need for laboratory studies on the roles of additional factors such as fluid chemistry, large displacements, higher concentrations of phyllosilicates, and time-dependent fault healing.

### Introduction

Shearing in crustal fault zones occurs through a complex combination of deformation processes. Near the Earth's surface (less than tens of kilometers depth), low temperature and confining pressure are thought to ensure that cataclastic flow dominates the shearing process. However, at greater depths, elevated temperatures and elevated confining and fluid pressures (i.e., hydrothermal conditions, in the case of aqueous pore fluids) give rise to a host of deformation mechanisms that may accompany or replace cataclastic flow. Shear strength may be lowered (or deformation rate increased) by subcritical crack growth, solution-

precipitation creep, and intracrystalline plastic flow [Tullis and Yund, 1980]. Alternatively, shear strength may be raised by time-dependent compaction, crack sealing, and asperity welding through crack healing and sintering of granular materials such as fault gouge [e.g., Fredrich and Evans, 1992]. Pore fluids accelerate each of these mechanisms [e.g., Lockner and Evans, this issue], generally by providing a pathway for the diffusive or advective transfer of solutes (e.g., pressure solution) or by participating in chemical reactions (e.g., stress corrosion). The rate and importance of these mechanisms, as well as the shearing strength, can therefore be expected to vary with temperature, strain rate, fluid and rock chemistry, fluid pressure, and effective pressure. Because both brittle and plastic deformation mechanisms are active, deformation can be described as transitional, and the strength of fault zones at these depths is probably poorly predicted by constitutive laws formulated for purely brittle or purely plastic mechanisms (e.g., “Byerlee's law” [Byerlee, 1978] and power law flow [Brace and Kohlstedt, 1980], respectively).

This paper is not subject to U.S. copyright. Published in 1995 by the American Geophysical Union.

Paper number 95JB00862.

At low temperatures the first-order frictional strength of rocks is approximately

$$\tau = \mu(\sigma_n - P_p) = \mu \cdot \bar{\sigma}_n \quad (1)$$

which specifies that the shearing stress  $\tau$  is a linear function of the effective normal stress  $\bar{\sigma}_n$  (normal stress  $\sigma_n$  reduced by the pore fluid pressure  $P_p$ ). For nearly all of the rock types studied, the coefficient of friction  $\mu \equiv \tau/\bar{\sigma}_n$  falls roughly in the range 0.60 to 0.85 [Byerlee, 1978], except for materials rich in phyllosilicates, in particular the expanding clays [Bird, 1984; Morrow et al., 1992] and the lizardite polymorph of serpentine [Reinen et al., 1991, 1994]. Under dry conditions or at low temperatures the effects of slip rate, temperature, and normal stress on  $\mu$  are modest and can be ignored in many applications. However, these second-order dependencies can be of considerable importance in controlling the stability of frictional slip. Slip will be unstable (stick-slip) if the strength of the fault decreases with slip at a rate exceeding the unloading rate of the surroundings. Theoretical analyses show that this criterion may be met when friction has a negative dependence on slip rate ("velocity weakening") [Dieterich, 1978; Ruina, 1983; Rice and Ruina, 1983; Tullis, 1988]. The recognition of a link between the velocity dependence of friction and the stability of sliding has led to the measurement of velocity dependence for a wide range of rock materials and conditions. Laboratory-derived friction constitutive laws that include velocity dependence have been used to construct numerical models of earthquake nucleation, earthquake cycles and seismicity [e.g., Tse and Rice, 1986; Stuart, 1988; Tullis, 1988; Dieterich, 1986, 1992; Rice, 1993; Ben-Zion and Rice, 1995 this issue]. These constitutive laws have been extended to include the second-order dependencies of friction on normal stress [Linker and Dieterich, 1992; Dieterich and Linker, 1992] and temperature [Chester, 1988, 1994, this issue; Chester and Higgs, 1992]. Despite these developments, only a few studies have examined the dependence of the friction of silicates on slip rate and temperature at hydrothermal conditions.

Two studies have examined the friction and velocity dependence of friction for heated dry granite. Stesky [1974, 1975, 1978a,b] loaded intact cylinders of granite and other crystalline rocks at room temperature until they failed, then heated the samples to as much as 700°C and continued shortening, causing slip on the inclined fracture surface. A few tests were also done on samples with a bare, inclined sawcut. At confining pressures up to 600 MPa (normal stresses up to 900 MPa), he observed unstable sliding from 25° to 300°C and stable sliding from 300° to 700°C. Frictional strength was insensitive to temperature up to at least 600° and decreased slightly at 700°C, though the data show much scatter. The friction of gabbro, quartzite and other rocks began decreasing at lower temperatures than did the friction of granite [Stesky, 1974].

Lockner et al. [1986] (hereafter referred to as LSB) shortened granite cylinders containing an inclined sawcut separated by a thin layer of simulated gouge (granite powder). Confining pressure was 250 MPa (normal stresses 380 to 460 MPa), and temperatures ranged from 22° to 845°C. They observed stable sliding in nearly all tests; exceptions were oscillatory slip at 200° and isolated stick-slip events associated with imposed steps in slip rate at 130° and 273°C. Friction generally increased with temperature over the entire range measured. LSB suspected this positive temperature dependence to be an artifact of the measurement procedure, a point we will discuss in more detail later.

Both Stesky [1975, 1978a] and LSB measured the velocity dependence of friction by imposing step changes in the remote loading rate while holding temperature fixed. In stable-sliding tests (i.e., the only type of tests in which velocity dependence could be measured) both reported a small, positive velocity dependence (velocity strengthening), roughly from 0 to 2% change in friction per decade change in slip velocity. Tse and Rice [1986] have interpreted stick-slip in Stesky's tests below 300°C as evidence for negative velocity dependence (velocity weakening), although this disagrees with near-zero velocity dependence reported by LSB at those temperatures.

Two studies of friction at hydrothermal conditions are worth noting here. Moore et al. [1986a,b] measured the strength of illite "gouge" in a series of triaxial sawcut tests at constant effective confining pressure of 100 MPa. Constant-slip-rate tests were done at 200°, 400°, and 600°C, at pore water pressures ranging from 0 to 100 MPa, and at sliding rates of 4.8 and 0.048  $\mu\text{m/s}$ . The tests showed no velocity dependence of friction at 200°C, but a negative dependence at 400° and 600°C in tests with  $P_{\text{H}_2\text{O}} \geq 10$  MPa. Moore et al. [1986a] surmised that velocity weakening resulted from two factors: strength at high temperatures and low slip rate may have been increased by lithification; and strength at high temperatures and high slip rate may have been decreased by fluid overpressure resulting from compaction and dewatering reactions of illite.

Higgs [1981] sheared layers of ultrafine quartz powder in triaxial sawcut tests at 150 MPa effective pressure. Constant slip rate and slide-hold-slide (stress relaxation) tests were done at 25°, 300°, 450°, and 600°C, at pore water pressures of 0 and 100 MPa, and at constant sliding rates of 4.65  $\mu\text{m/s}$  (dry) and 0.465  $\mu\text{m/s}$  (wet). The friction coefficient at constant slip rate showed only minor variations with either temperature or pore pressure. However, tests with 100 MPa pore  $\text{H}_2\text{O}$  pressure and temperatures  $\geq 300^\circ$  showed substantial weakening during relaxations to shear strain rates  $\approx 10^{-3}$  to  $10^{-6} \text{ s}^{-1}$  (slip rates  $\approx 0.2$  to  $0.0002 \mu\text{m/s}$ ), while dry tests, and all tests at 23°, did not show this weakening. Veins, porosity reduction and other evidence for solution transport deformation were seen in samples from the former, but not the latter, tests. Chester and Higgs [1992] inferred that slip in Higgs' tests at 300° and 450°C at moderate slip rates involved both cataclastic flow and solution transport creep, while those at 600°C and low slip rates involved creep alone.

Previous studies have not directly measured strength and velocity dependence at hydrothermal conditions. Therefore we have performed a suite of shearing experiments on laboratory "faults" in granite over a wide range of conditions in order to examine the effects of temperature,  $\text{H}_2\text{O}$  fluid pressure, and slip rate on shear strength and the stability of sliding (steady slip versus stick-slip). The principal suite of experiments was performed with pore  $\text{H}_2\text{O}$  pressure,  $P_{\text{H}_2\text{O}} = 100$  MPa ("wet") and temperatures up to 600°C. Results are combined with those of LSB for similar tests on dry granite gouge to 845°. Preliminary findings were reported by Blanpied et al. [1991]. Constitutive parameter values are reported in a separate paper (M.L. Blanpied et al., manuscript in preparation, 1995). Westerly granite was chosen for this study because a substantial literature exists on its frictional properties.

## Experimental Methods

The sliding experiments reported in the present paper (Table 1) were conducted in a triaxial apparatus using argon gas as a confining medium. See LSB and Blanpied et al. [1991] for addi-

Table 1. Experiments on Wet Granite Gouge

Experiment	Temp, <sup>a</sup> °C	$P_{H_2O}$ , MPa	Preheat Time, <sup>b</sup> hours:min	Jacket Thickness, mm	Bore hole <sup>c</sup>	Slip Velocities, $\mu\text{m/s}$	Axial Displacement, mm
HWGG3	23	100	–	0.25	blind	1, 0.1	2.85
HWGG14	23	100	–	0.25	blind	1, 0.1	3.49
HWGG19	100	100	1:15	0.25	blind	1, 0.1	2.81
HWGG11	150	100	1:10	0.25	blind	1, 0.1	2.77
HWGG10	200	100	1:00	0.25	blind	1, 0.1	2.61
HWGG24	200	100	1:00	0.38	blind	1, 0.1	3.38
HWGG43	200	100	4:50	0.38	blind	0.1, 0.01	3.46
HWGG48	225	100	2:52	0.38	through	1, 0.1	3.16
HWGG20	250	100	4:16	0.38	blind	0.1, 0.01	3.01
HWGG21	250	100	1:20	0.38	blind	1, 0.1	3.55
HWGG22	250	100	1:03	0.38	blind	1, 0.1	3.88
HWGG23	250	100	1:03	0.25	blind	1, 0.1	2.70
HWGG49	275	100	1:35	0.38	through	1, 0.1	3.32
HWGG12	300	100	1:00	0.25	blind	1, 0.1	3.05
HWGG26	300	100	0:55	0.38	blind	1, 0.1	3.36
HWGG27	300	100	1:00	0.38	blind	1, 0.1	3.21
HWGG9	350	100	0:55	0.25	blind	1, 0.1	3.21
HWGG18	350	100	4:40	0.38 <sup>d</sup>	blind	0.1, 0.01	4.12
HWGG16	400	100	1:00	0.25	blind	1, 0.1	3.17
HWGG15	450	100	0:35	0.38 <sup>d</sup>	blind	1, 0.1	4.12 <sup>e</sup>
HWGG17	450	100	25:00	0.38 <sup>d</sup>	blind	1, 0.1	3.65
HWGG28	450	100	4:20	0.38	blind	0.1, 0.01	3.22
HWGG7	500	100	1:15	0.25	blind	1, 0.1	3.68
HWGG38	600	0	1:48	0.38	blind	1, 0.1	4.56
HWGG36	600	10	1:24	0.38	blind	1, 0.1	3.65
HWGG8	600	100	1:05	0.25	blind	1, 0.1	3.36
HWGG42	600	100 <sup>f</sup>	2:40	0.25	through	0.1	3.35

Effective normal stress = 400 MPa.

<sup>a</sup> Peak temperature.

<sup>b</sup> Interval between reaching peak T and initiating axial loading.

<sup>c</sup> "Through" holes intersected the sliding surface; "blind" holes ended ~3 mm from it.

<sup>d</sup> Cu jackets used in these experiments were not annealed.

<sup>e</sup> Experiment was stopped before rupture of the copper jacket.

<sup>f</sup> Pore pressure was stepped between 0 and 100 MPa after 2.1 mm axial displacement.

tional details on the apparatus and methods. Our tests were designed to be similar to those on dried granite gouge by LSB. Cylinders (19 mm diameter x ~38 mm long) of Westerly granite (Figure 1) contained a sawcut surface cut at 30° to the loading axis. Sawcut surfaces were ground flat, then roughened slightly by grinding on a glass plate with number 240 SiC powder and water. The sawcut contained a layer of simulated fault gouge (granite powder, particle sizes  $\leq 90 \mu\text{m}$ , initial thickness 0.58 mm). Samples were jacketed against confining pressure with thin sleeves of Cu (0.25 mm or 0.38 mm thick). Copper jackets were annealed before use in all but three cases (Table 1). In most experiments a blind hole in the upper sample half and in the upper assembly pieces allowed access for pore water and for a thermocouple used to control temperature. In a few experiments this hole was extended to intersect the sliding surface and filled with coarse quartz sand to prevent the loss of gouge from the surface.

Temperature was measured within the upper bore hole. Temperatures quoted in this paper refer to the peak temperature in the sample. Because of the design of the single-zone resistance furnace, temperatures at the upper and lower end of the sawcut were down approximately 15% and 8%, respectively, from the peak temperature, which was located near the center. Temperatures were generally held constant to within 2°C or better during sliding.

At the start of each test,  $P_c$  was raised to 400 MPa. A vacuum was drawn on the pore pressure system and sample, then distilled

water was introduced into the evacuated system and raised to the run pressure of 100 MPa. We rely on flow of water under pressure to saturate the granite sample. Both  $P_c$  and  $P_{H_2O}$  were held constant by servo control. Temperature was raised at a rate of approximately 10°C/min to the run value, then held constant for  $\geq 1$  hour (exact time given in Table 1). Axial load was increased by advancing the piston against the end of the sample column. With increasing axial load, effective normal stress across the sawcut ( $\bar{\sigma}_n \equiv \sigma_n - P_{H_2O}$ ) increased from the initial value of 300 MPa. Once  $\bar{\sigma}_n$  reached 400 MPa (at  $\tau/\bar{\sigma}_n = 0.432$ ), it was thereafter held constant by servo controlled adjustment of  $P_c$ . This point is marked on plots of  $\mu$  versus displacement as a slight increase in steepness of the loading slope. The real-time calculation of normal stress accounted for the change of fault area with slip and for the confining-pressure-dependent piston seal friction. Real time calculations of stress took into account the decrease in nominal area of contact across the sliding surface with slip and the pressure dependence of the piston seal friction.

To measure the velocity dependent response, the axial shortening rate was stepped periodically by factors of 10 after every 0.5 mm of axial displacement, beginning at 2.0 mm. Axial rates were chosen such that the displacement rate resolved onto the plane of the sawcut,  $V$ , was stepped between 1.0 and 0.1  $\mu\text{m/s}$  ("standard" tests), or between 0.1 and 0.01  $\mu\text{m/s}$  ("slow" tests). (For reference, 0.01  $\mu\text{m/s} = 315 \text{ mm/yr}$  and represents a gouge-thickness-averaged shear strain rate of about  $10^{-5} \text{ s}^{-1}$ ). The experiments

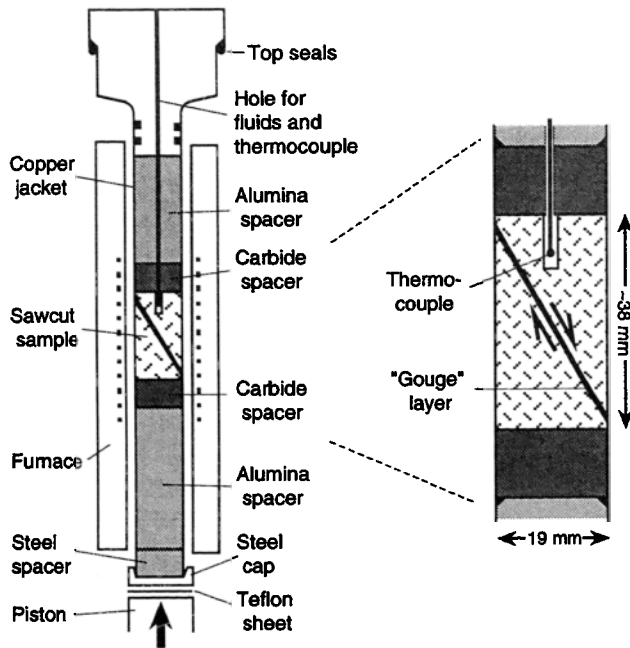


**Figure 1.** Cross-section view of sample configuration used in triaxial sliding experiments. The same configuration was used in tests on dry granite gouge by *Lockner et al.* [1986]. A granite cylinder contains a sawcut at  $30^\circ$  to the sample axis filled with  $\sim 0.5$  mm of gouge (granite powder). Axial shortening of the assembly causes shearing of the gouge-filled sawcut. The sample, along with spacers of alumina and tungsten carbide, are contained within a thin, copper jacket which is silver-soldered at the lower end. An axial hole provides access for pore fluid and for a thermocouple used in the temperature control servosystem. The entire jacketed assembly rests inside a resistance furnace. Space between the sample assembly and furnace wall is loosely packed with boron nitride powder and silica wool to hinder convection of the confining pressure gas but to allow the lower half of the assembly to shift sideways. The lower end of the assembly is capped by a steel disk; a thin sheet of lubricated Teflon allows the interface between the disk and the steel piston to slide easily.

ended with rupture of the jacket after two to five velocity steps, at an axial displacement of 2.6 to 4.1 mm and a total slip on the sawcut of 1.8 to 3.1 mm.

A total of about 30 experiments were performed at temperatures ranging from  $23^\circ$  to  $600^\circ\text{C}$  (Table 1). We limited temperature to  $600^\circ\text{C}$  in order to avoid the possibility of partial melt. LSB ran experiments on dry samples at a constant confining pressure of 250 MPa rather than constant normal stress, resulting in a time-varying normal stress in the range 380 to 460 MPa during the velocity-stepping portion of their experiments. They imposed decade velocity steps in the range 0.055 to 5.5  $\mu\text{m/s}$  after every 0.5 mm of axial displacement, beginning at 1.5 mm.

The velocity dependence of friction was estimated by measuring the long-term change in friction,  $\Delta\mu_{ss}$ , that resulted from each velocity step, relative to a strain hardening or softening trend (see LSB and Figure 10 inset). The measurements are normalized by the change in  $\ln V$ , and given here as values of  $\partial\mu_{ss}/\partial\ln V$  ( $\approx \Delta\mu_{ss}/2.303$  for decade steps in  $V$ ). In recent literature the quantity  $\partial\mu_{ss}/\partial\ln V$  is often termed  $a-b$ , reflecting the wide use of a velocity-dependent friction constitutive law as formulated by *Ruina* [1980, 1983]. Measurements of  $\partial\mu_{ss}/\partial\ln V$  from some tests (those with run names through HWGG27) were presented by *Blanpied*

*et al.* [1991]. The largest uncertainty in the values of  $\partial\mu_{ss}/\partial\ln V$  comes from ambiguity in choosing  $\mu_{ss}$  before and after velocity steps, in the presence of work-hardening trends in the friction-displacement curves. This introduces an uncertainty of  $\sim 0.0003$  to 0.0005 into all but the most well-behaved measurements. In wet runs at  $>350^\circ\text{C}$  the 0.5 mm of slip between velocity steps was not sufficient to achieve steady state sliding (see Figure 3c), introducing a larger uncertainty; corresponding measurements likely represent rough lower bounds on the magnitude of  $\partial\mu_{ss}/\partial\ln V$ .

Values of  $\mu$  and values of  $\partial\mu_{ss}/\partial\ln V$  have been corrected for the velocity dependence of the piston seal friction. The piston seal consists of an O-ring which seats against a bronze ring of triangular cross section. Pressure transmitted by the O-ring contracts the bronze ring against the polished and lubricated steel piston. We believe that most of the sliding resistance of the piston seal comes from the bronze/steel contact, rather than from the O-ring itself. The piston seal friction was measured to a precision of  $\sim 0.0003$  (friction units) at the beginning of each experiment by stepping the rate of advance of the piston before it contacted the sample assembly. On average, this correction reduced values of  $\partial\mu_{ss}/\partial\ln V$  by an amount  $0.00053 \pm 0.00018$ .

Values of  $\mu$  have also been corrected for the contribution to measured strength of the copper jacket. Jacket strength was determined by performing room temperature sliding tests on cylindrical steel samples containing a polished  $30^\circ$  sawcut separated by a thin sheet of lubricated Teflon. By performing tests with various thicknesses of copper jacket, we were able to remove the contribution of the Teflon/steel surface from the measured strength, leaving a jacket strength that depends linearly on thickness. We calculate that at room temperature and  $\bar{\sigma}_n = 400$  MPa, the 0.25-mm-thick jackets contribute 0.0162 to the apparent coefficient of friction; 0.38-mm-thick jackets contribute 0.0243. Annealed jackets work hardened to a strength equal to unannealed jackets in less than 1 mm slip. No rate dependence of jacket strength was discernible in our tests, making the upper bound on the contribution to  $\partial\mu_{ss}/\partial\ln V$  roughly 0.0002. Jacket strength at elevated temperatures was estimated using a relation from *Higgs* [1981]; combining this relation with our room temperature determinations, we calculate that jacket strength falls with increasing temperature and is negligible above  $400^\circ\text{C}$ . Friction values displayed in scatter plots in this paper have been corrected accordingly, and we have also applied this correction to friction data from Figure 4 of LSB.

Most deformed samples were left in their copper jackets for the preparation of optical thin sections. These samples were vacuum-impregnated with epoxy, and doubly polished 35- $\mu\text{m}$ -thick sections were cut parallel to the sample axis and perpendicular to the sawcut. For the remaining samples, the sliding surfaces were directly examined with a hand lens. In this case the two sample halves were separated by hand, which generally left the gouge layer attached to one or both rock surfaces.

Before presenting results, we must add two notes of caution. First, slip in these experiments is limited to a few millimeters (gouge-thickness-averaged engineering shear strains of roughly 4 to 7). For this reason, values of strength and velocity dependence may not represent a true steady state condition. For example, the physical properties of the gouge evolve with increasing displacement due to ongoing comminution, compaction, and possibly chemical reactions. Evidence for this evolution is seen by the presence of work-hardening or -weakening trends in most runs. Earlier work on granite at room temperature has shown that values of  $\partial\mu_{ss}/\partial\ln V$  and  $D_c$ , the characteristic evolution displace-

ment, evolve downward with slip, reaching fairly steady levels only after 5 to 10 mm [Dieterich, 1981; Biegel et al., 1989; Weeks et al., 1990; J. Byerlee, unpublished data, c. 1988], although this trend is not always seen in triaxial tests [Lockner and Byerlee, 1986; LSB; Marone et al., 1990]. Furthermore, tests to even higher displacements at room temperature have shown that  $\partial\mu_{ss}/\partial\ln V$  continues to evolve even after 50–100 mm [Weeks et al., 1990]. The physical basis of these various displacement-dependent changes are not completely understood; therefore we will not speculate about the effect that further slip would have on our results at elevated temperature.

Second, shearing of the gouge layer is accompanied by changes in gouge volume in response to increasing displacement or changing velocity [Morrow and Byerlee, 1989; Marone et al., 1990; Lockner and Byerlee, 1994]. In our sample geometry with a blind bore hole, changes in gouge volume require flow of water through a thin region (~2–3 mm) of intact granite (Figure 1). Fluid pressure will remain equilibrated only if the changes in gouge volume occur sufficiently slowly and the granite permeability remains sufficiently high. Calibration experiments indicated that the characteristic time for pore pressure equilibration is of the order of 100 s. For changes in gouge volume that occur over times shorter than this, some transient changes in pore fluid pressure are expected. For example, if an increase in slip rate causes the gouge to dilate, pore pressure will fall causing an increase in strength. At our fastest rate of 1  $\mu\text{m/s}$ , the characteristic time for pressure equilibration is comparable to the time required to slide the characteristic weakening displacement (tens to hundreds of micrometers). Therefore determination of transient constitutive parameters (M.L. Blanpied et al., manuscript in preparation, 1995) may be affected in some cases. This bias should be most pronounced for upward velocity steps from 0.1 to 1  $\mu\text{m/s}$  in "standard" tests. Measurements of residual friction and of steady state velocity dependence should not be affected.

The permeability of intact granite may be reduced by redistribution of material in solution. We have presented elsewhere [Blanpied et al., 1992] experiments in which intact granite near a gouge-filled sawcut became sealed, effectively separating the pore fluid in the deforming gouge layer from the external pore pressure control system. These experiments showed extremely low shear strength, interpreted to result from undrained compaction of the sealed gouge layer which lowered the effective stress. Below we demonstrate that self-sealing in our experiments is limited to slow, wet experiments at greater than 500°C, conditions that we have excluded from the present study for that reason. While we are confident that pore pressure communication was maintained in all experiments presented here (see discussion below), partial reduction of the granite permeability from solution-transport may increase the magnitude and/or persistence of the transient pore pressure changes mentioned above.

## Experimental Results

### Sample Observations

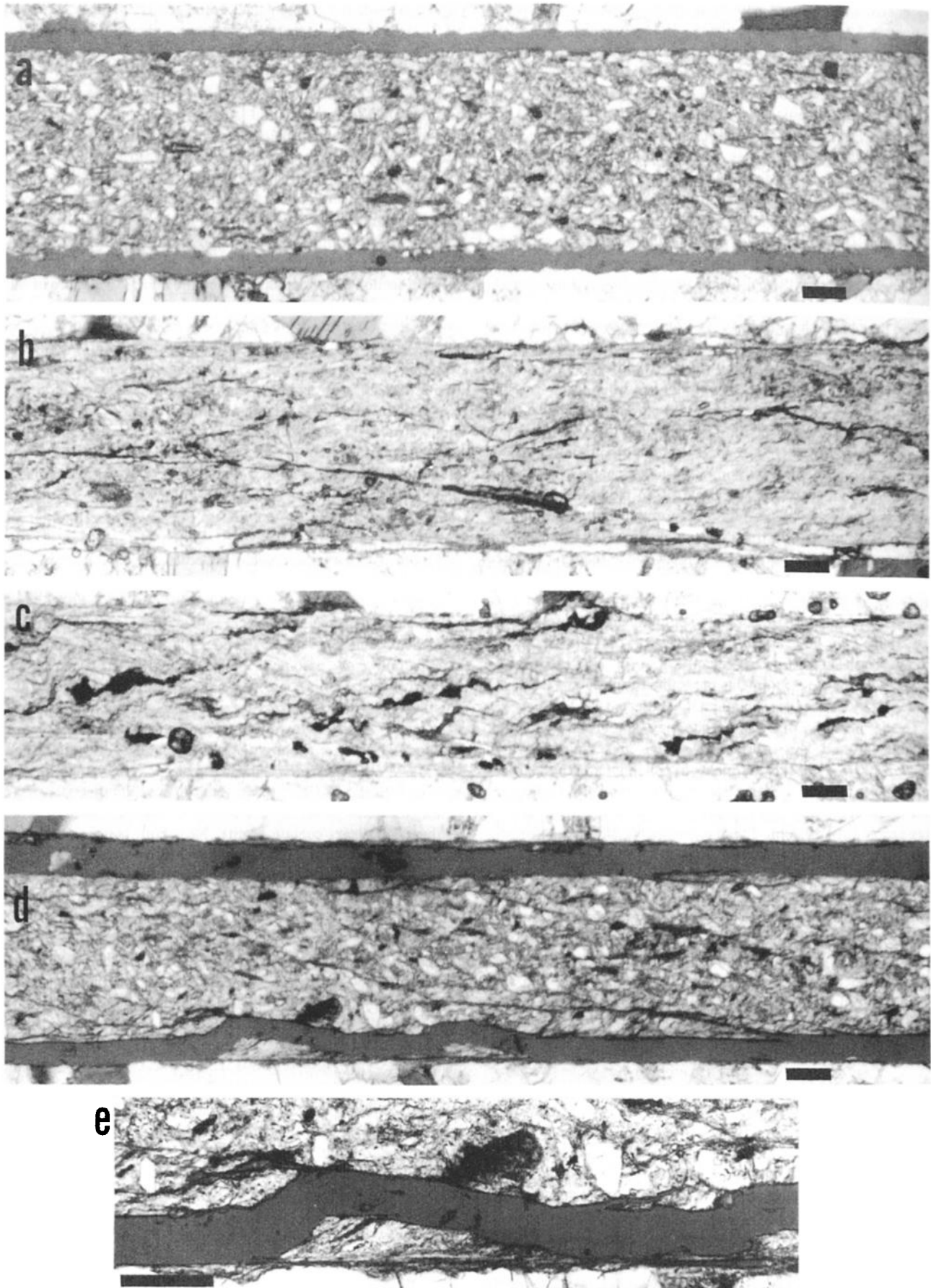
Examination of the samples with a hand lens showed that the gouge layers, which began as a loose powder, became compacted and indurated to varying degrees at all conditions tested. At lower temperatures (<400°C) the gouge retained its light gray color and separated easily from the granite surfaces, which appeared nearly undisturbed. Coherent flakes of compacted gouge could be removed from the sliding surfaces without crumbling. These flakes could easily be broken apart on planes shallowly dipping in the

direction of sliding. These planes correspond to the  $R_1$  orientation of Riedel shears and presumably represent planes of localized deformation within the gouge [Tchalenko, 1970; Logan et al., 1970; Byerlee and Savage, 1992; Lockner and Byerlee, 1993].

At higher temperatures (450° to 600°C) the surfaces of gouge flakes were a darker gray and lacked obvious  $R_1$  shears, and the gouge was somewhat difficult to remove from the granite surfaces. Where the gouge was removed, the surfaces of both the gouge and the rock were smooth and somewhat shiny, as if polished. Thin section examination (see below) suggests that the polished appearance resulted from localized shearing and extreme comminution within a narrow zone or surface immediately adjacent to the gouge-rock interface.

Thin section examination revealed the internal structure of the gouge layers. Figure 2a shows the initial condition of the gouge layer before shearing. This sample was taken to conditions ( $P_c = 400$  MPa,  $P_{H_2O} = 100$  MPa, 550°C), held for about 80 min, and removed due to a jacket leak. The photomicrograph illustrates the initial rock surface roughness and the particle shape and size distribution in the gouge. A large number of particles have dimensions of tens of micrometers. Quartz and feldspar particles are angular and subequant in dimension; biotite laths (difficult to see at the scale of the micrograph) typically have aspect ratios of 1:5 and are mostly aligned subparallel to the sawcut. The preferred shape orientation of biotite grains presumably resulted from compaction of the gouge layer.

Figure 2b shows a sample deformed at 150°C. Comparison to Figure 2a shows that the gouge has been pervasively sheared. There is a marked decrease in the number of large particles, and abundant Riedel shears in the  $R_1$  (angled) and Y (interface-parallel) orientations are seen throughout the gouge layer. Some biotite particles have become elongated along Riedel shears, apparently by basal slip. Others have been finely divided and distributed throughout the gouge layer. This microstructure is typical of gouges from dry tests from room temperature to 845°C (Figure 2c) and wet tests to about 400°C. In contrast, gouge deformed wet at 600°C retains a distribution of particles sizes similar to the starting material (Figure 2d). Several distinct  $R_1$  shears are seen cutting the entire gouge layer, but they are widely spaced; several of these  $R_1$  shears contain biotite. Near both gouge-rock interfaces, localized deformation is indicated by narrow, boundary-parallel shears. It appears that much of the deformation in this experiment occurred by slip near the gouge-rock interfaces, with relatively little internal deformation of the gouge layer. Figure 2e is a closer view of a preserved boundary shear. The shear is planar, roughly 5 to 10  $\mu\text{m}$  wide, and is located such that it is in contact with the most elevated topography on the rough granite surface. Depressions in the granite are filled with gouge. This in-filling of topography on the rock surface and tendency to separate along the boundary shear accounts for the shiny appearance of that surface when viewed by eye. Under plane polarized light the boundary shear is slightly pleochroic, and under crossed polarizers it reveals a strong crystallographic preferred orientation. These two observations suggest that the boundary shear is rich in biotite oriented with basal plane subparallel to the plane of the shear. We note, however, that pure quartz powder deformed under similar conditions also developed a preferred orientation [Higgs, 1981]. Also, Power and Tullis [1991] observed strong crystallographic preferred orientation in ultrafine quartz on slickensided fault surfaces in the Dixie Valley normal fault zone, Nevada. Although the relevant fault slip occurred at a depth of <2 km and a temperature of  $\leq 270^\circ\text{C}$ , Power and Tullis concluded





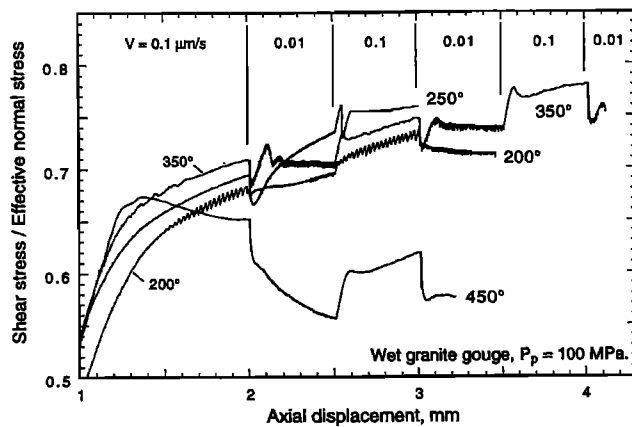


Figure 4. Friction displacement curves for "slow" runs (0.01 and 0.1  $\mu\text{m/s}$ ) with granite gouge at  $\sigma_n = 400$  MPa and  $P_{\text{H}_2\text{O}} = 100$ . Data averaged over 25-s intervals for plotting.

creasing temperature from strain hardening below  $\sim 350^\circ\text{C}$  to strain weakening and decreased strength above  $\sim 400^\circ\text{C}$  (above  $\sim 350^\circ\text{C}$  in slow runs, Figure 4). The direct response shows an abrupt increase at  $\sim 250^\circ\text{C}$ : At temperatures  $\leq 225^\circ\text{C}$ , strength transients are small and short-lived, while at temperatures  $\geq 250^\circ\text{C}$  the direct change in friction is more pronounced and the subsequent evolution toward steady state is more protracted.

**Coefficient of friction.** Following LSB, we compare the strengths of different runs by measuring the coefficient of friction at 2.9 mm axial displacement. This displacement was chosen because by then most of the strain hardening or softening had occurred, and yet most jackets had not ruptured. In most cases, 2.9 mm corresponded to slip at the higher of two rates (see Figure 3). We extrapolated the friction-displacement traces in order to also obtain a measurement of strength at 2.9 mm and the lower slip rate. Repeated experiments showed excellent reproducibility of strength and the response to velocity steps.

Coefficient of friction is plotted vs. temperature in Figure 6. Dry runs generally show an increase in strength with temperature above  $200^\circ\text{C}$ . Wet runs show an increase in strength from  $23^\circ$  to about  $300^\circ\text{C}$  and falling strength at higher temperatures. The strength measured in dry runs and in wet runs at low temperatures may be biased to low values because of the small displacement possible in our apparatus. Strain hardening was seen in most tests, likely due to progressive compaction of the gouge during shearing and particle size reduction, consistent with direct observations of volumetric strain in sliding tests on gouge [Marone et al., 1990; Scott et al., 1994]. Compaction processes are likely to operate more rapidly at higher temperatures and with pore fluid [Lockner and Evans, this issue; Dewars and Hajash, this issue], so the compaction state may differ between samples deformed to the same slip at different temperatures. More displacement would be needed to define the peak strength of strain-hardening samples, and the corresponding values plotted in Figure 6 are lower bounds. The temperature dependence of strength for wet gouge below  $400^\circ\text{C}$  may be biased for a similar reason. Tests to larger displacement, or temperature-stepping tests, will be required to resolve this point. Nonetheless, above  $\sim 300^\circ\text{C}$ , wet gouge clearly exhibits a negative temperature dependence.

**Effects of  $P_{\text{H}_2\text{O}}$ .** In Figure 7 we show friction-displacement curves from three runs with different pore pressure. All three runs were done at  $600^\circ\text{C}$  and at the same constant effective normal

stress of 400 MPa. The sample marked "dried" was vacuum dried during heating and resting at  $600^\circ$  for  $\sim 1$  hour, then was vented to the atmosphere during deformation. The coefficient of friction in the dried run was about 0.8, in agreement with the results of LSB. Velocity steps caused a strength transient but almost no change in steady state friction level. With the addition of 10 MPa  $P_{\text{H}_2\text{O}}$  the friction at the higher slip rate is nearly unchanged, but the friction at the lower slip rate is depressed by 0.015 to 0.025 compared to the dry run. With 100 MPa  $P_{\text{H}_2\text{O}}$  the friction is depressed at both rates, though much more so at the slower rate. Velocity steps are followed by a prolonged evolution of strength containing multiple reversals.

Decreased strength at hydrothermal conditions suggests the possibility that pore fluid became overpressured within some samples. If fluid pressures within the gouge layer became higher than the 100 MPa measured in the external fluid pressure system, this would decrease the effective stress and thus decrease the apparent coefficient of friction which is calculated assuming no overpressure. In fact, this did occur in experiments performed at the most extreme conditions: temperatures of  $550^\circ$  and  $600^\circ\text{C}$  and  $V \leq 0.1 \mu\text{m/s}$ , as described by Blanpied et al. [1992]. In the present paper we have excluded slow runs at  $500^\circ$  and above and next demonstrate with reference to Figure 8 that fluid overpressure did not occur in our other experiments.

The self-sealing experiments described by Blanpied et al. [1992] showed anomalously low strength. To briefly summarize their findings, experiments at  $550^\circ$ - $600^\circ\text{C}$  and  $V = 0.1 \mu\text{m/s}$  showed elastic loading to a modest peak shear stress, followed by a rapid (but aseismic) decay in strength to the remarkably low apparent level of  $\mu = 0.22$  (Figure 8, run HWGG31). Imposed steps in the externally controlled pore pressure did not alter the shear stress, showing that there was no fluid communication between the bore hole and the fault surface. Blanpied et al. concluded that the fluid pathway between the blind bore hole and the fault surface (see Figure 1) became sealed by the redistribution of materials in solution during the long period of time at high temperature preceding slip (4 to 5 hours preheat,  $\sim 3$  hours loading). Apparently, compaction of the undrained gouge layer raised the pore pressure to  $\sim 300$  MPa, resulting in low shear strength.

We compare the self-sealed tests with three other experiments, all performed at  $600^\circ\text{C}$  (Figure 8). A standard run (HWGG8)

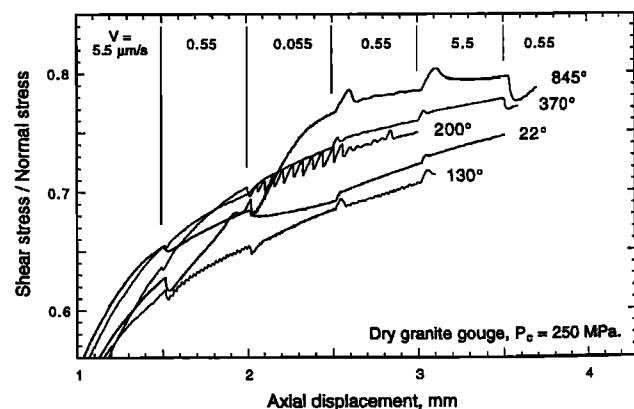
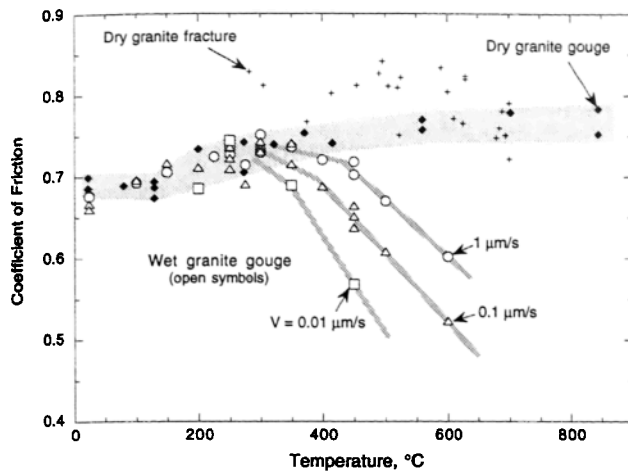


Figure 5. Friction displacement curves for selected runs on dried granite gouge at  $P_c = 250$  MPa from Lockner et al. [1986]. Data collected once per second and averaged over 1- $\mu\text{m}$  intervals for plotting. The slight oscillations seen most prominently in the run at  $130^\circ$  are due to cyclic variations in temperature of  $\leq 3^\circ\text{C}$ .



**Figure 6.** Friction versus temperature measured at 2.9 mm axial displacement for wet granite gouge at  $\bar{\sigma}_n = 400$  MPa,  $P_{H_2O} = 100$  MPa, and three slip rates (open symbols). Also shown are data from sliding tests on dry granite gouge from *Lockner et al.* [1986, Figure 5] ( $\sigma_n = 380$  to 460 MPa) and from sliding tests on dry, prefractured granite from *Stesky* [1975] ( $\sigma_n = 370$  to 450 MPa). Ambiguities in the strength measurements for wet gouge are generally less than the symbol size. Values for wet gouge and for dry gouge from Lockner et al. have been corrected for the temperature-dependent strength contribution from the copper sample jackets. Gray shading and lines are drawn as guides to the eye.

showed the much higher strength of  $\mu \approx 0.52$  at  $V = 0.1 \mu\text{m/s}$ . The other two experiments were performed on altered samples, in which the bore hole was extended to intersect the sawcut surface. The first sample (also described by *Blanpied et al.* [1992]) contained a layer of simulated gouge (HWGG42). A high initial strength was followed by rapid decay to a level of  $\mu \approx 0.46$ . Steps in pore pressure (not included in the figure) showed the expected response in this run, demonstrating that pore pressure in the gouge was being externally controlled. The second altered sample lacked a gouge layer (HWGG39). In this case the initial and residual strengths were nearly the same, and the residual friction was about 0.48. Note that in these three runs the residual friction fell in the narrow range 0.46 to 0.52.

On the basis of this comparison we conclude that the value  $\mu = 0.5$  is robust for the sliding of granite at  $600^\circ\text{C}$ ,  $V = 0.1 \mu\text{m/s}$ ,  $\bar{\sigma}_n \approx 400$  MPa, and  $P_{H_2O} = 100$  MPa. We also conclude that standard runs to our maximum temperature of  $600^\circ\text{C}$  did not become overpressured. We find evidence for self-sealing only in those experiments with the highest temperatures, longer preheat times, and slower sliding rates. Apparently, the shorter time spent at conditions in standard experiments ( $\sim 1$  hour preheat, 20–30 min loading) is insufficient to allow seal formation, even at  $600^\circ$ . Also, at temperatures below  $\sim 500^\circ\text{C}$ , the kinetics of solution transport are too slow to allow a pressure seal to form even for the longer duration of our slow tests. To test this last point, we repeated a standard experiment at  $450^\circ\text{C}$ , extending the usual 1-hour preheating time to 25 hours. The extended preheating caused a small increase in the initial strength of the gouge, but that difference did not persist (Figure 9). We conclude two points from this comparison: first, that a seal does not form at temperatures at or below  $450^\circ$ , even for times of up to 25 hours; and second, that the response of samples to velocity steps does not depend critically on the preheating time, at least for the range of times and temperatures explored here.

Samples preheated at high temperature and long times showed an initial peak strength. For example, gouge-filled samples deformed at  $600^\circ\text{C}$  showed a initial peak (Figure 8, runs HWGG8, HWGG42), although the initially bare sample did not (HWGG39). (While the self-sealed sample, HWGG40, also showed an initial peak, the effective stress at the time the peak was reached is unknown.) Note also that the sample preheated at  $450^\circ$  for 25 hours showed a small peak not seen in the standard run at that temperature (Figure 9). We infer that the gouge layer becomes lithified during the preheating interval, most likely from time-dependent compaction of the gouge, or from asperity welding through sintering. For example, *Lockner and Evans* [this issue] showed that quartz powder compressed at hydrothermal conditions undergoes initially rapid compaction followed by compaction at a reduced rate. Our observations of time-dependent strengthening are consistent with those of *Fredrich and Evans* [1992], who preheated samples containing a layer of simulated quartz gouge at  $600^\circ\text{C}$ , then measured sliding resistance at a reduced temperature. Samples preheated with pore water pressure showed a high initial strength, whereas those preheated dry, and those not preheated at all, showed no initial peak. No difference in strength was found between samples held at  $600^\circ\text{C}$  for 1 min versus 2 hours. Similarly, our samples showed little difference in peak strength for preheat times of 1.1 hours (Figure 8, HWGG8) versus 2.7 hours (HWGG42). Following Fredrich and Evans, we infer that the majority of the strengthening occurred while heating to  $600^\circ$ , roughly 1 hour in both studies. (We must note, however, that *Chester and Higgs* [1992] found no evidence for time-dependent strengthening during stress relaxation tests on wet quartz powder at  $600^\circ\text{C}$ .)

**Velocity dependence of friction.** The velocity dependence of steady state friction,  $\partial\mu_{ss}/\partial\ln V$ , was measured for each velocity step, as described earlier and illustrated in the inset to Figure 10. The velocity dependence shows a pronounced and complex dependence on temperature. Values of  $\partial\mu_{ss}/\partial\ln V$  for wet gouge are plotted versus temperature in Figure 10a. In the standard tests (closed circles), velocity strengthening is seen at  $23^\circ$ ,  $250^\circ$  and above  $350^\circ\text{C}$ . Velocity weakening is seen from  $100^\circ$  to  $350^\circ$ , except at  $250^\circ$ . From  $350^\circ$  to  $600^\circ$ ,  $\partial\mu_{ss}/\partial\ln V$  rises from negative to

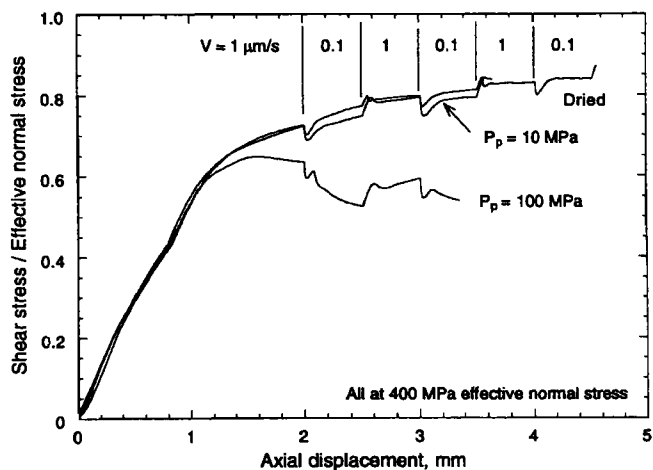


**Figure 7.** Friction displacement curves for granite gouge slid at  $600^\circ\text{C}$ ,  $\bar{\sigma}_n = 400$  MPa, and three different pore pressures. Elevated  $P_{H_2O}$  causes weakening even at constant effective stress. Weakening is more pronounced at the lower slip rate. The kink at  $\mu = 0.43$  results from the initiation of normal stress servo control.

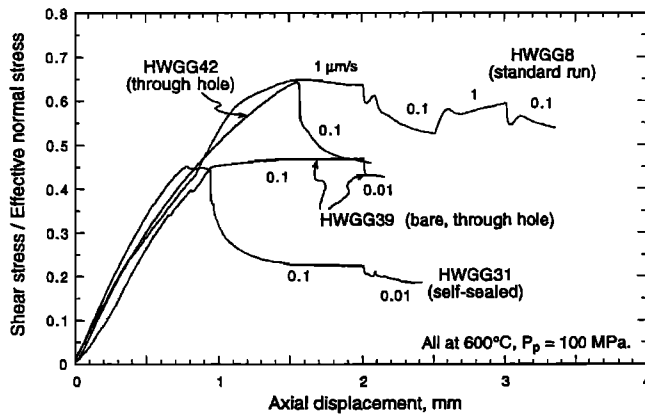


**Figure 8.** Friction displacement curves for four experiments on wet granite at 600°C. Small numbers show sliding velocity in  $\mu\text{m/s}$ . Experiment HWGG31 shows anomalously low strength because pore fluid was trapped and overpressured within the deforming gouge. Remaining three runs give a consistent strength of  $\mu \approx 0.5$  at  $V = 0.1 \mu\text{m/s}$ . See text for explanation.

strongly positive ( $>0.03$ ). The values at temperatures  $>350^\circ$  are lower bounds as explained earlier. (Note that, owing to oscillatory slip, values of  $\partial\mu_{ss}/\partial\ln V$  at 150° and 200°C (closed squares) were estimated from only  $\sim 0.2$  mm of slip following the first velocity step.) Also shown are values for wet quartz gouge reported by *Chester and Higgs* [1992]. Their values were determined by modeling slide-hold-slide relaxation tests with Ruina's law with one state variable (see below), rather than from velocity steps. While estimates of  $\partial\mu_{ss}/\partial\ln V$  from such modeling are probably less accurate, we note that they are in good agreement with our data.

Velocity dependence measurements from LSB for dried granite gouge are plotted in Figure 10b. Also shown are values for dry quartz gouge [*Chester and Higgs*, 1992] and dry, prefractured granite [*Stesky*, 1975]. Comparing Figures 10a and 10b shows that the presence of 100 MPa  $P_{\text{H}_2\text{O}}$  has a marked influence on  $\partial\mu_{ss}/\partial\ln V$ . At room temperature the addition of  $\text{H}_2\text{O}$  raises the value of  $\partial\mu_{ss}/\partial\ln V$  slightly, although the contrast is small and may not be significant. In the interval 100° to 350°C the addition of  $\text{H}_2\text{O}$  shifts  $\partial\mu_{ss}/\partial\ln V$  toward the negative, except at 250° and 275°C where the data are more positive and show considerable scatter. Above 350° the addition of  $\text{H}_2\text{O}$  increases the magnitude of  $\partial\mu_{ss}/\partial\ln V$  several-fold.

The influence of slip rate on  $\partial\mu_{ss}/\partial\ln V$  is seen by comparing the data from standard and slow tests on granite (Figure 10a, closed versus open circles). The slow test at 250°C showed velocity weakening, in contrast to the standard test at 250° but similar to the standard test at 300°. The slow test at 350° showed velocity strengthening, in contrast to the standard test at 350° but similar to the standard test at 400°. From these comparisons it is clear that for temperatures  $\geq 250^\circ\text{C}$ , decreasing the slip rate raises  $\partial\mu_{ss}/\partial\ln V$  and also lowers slightly the temperature of transition from velocity weakening to velocity strengthening.

Recent work has shown that observations of  $\partial\mu_{ss}/\partial\ln V$  can be affected by velocity-dependent changes in gouge porosity [*Morrow and Byerlee*, 1989; *Marone et al.*, 1990; *Beeler and Tullis*, 1995]. Specifically, the rate at which porosity changes with slip may depend on slip rate. This affects observations of  $\partial\mu_{ss}/\partial\ln V$  because the component of work done against confining stress thereby depends on velocity and is included in the measurement of  $\mu_{ss}$  [*Marone et al.*, 1990]. However, we do not have

the measurements of volumetric strain in the gouge needed to evaluate the magnitude of this effect.

## Interpretation of Observations

### Deformation Micromechanisms in Gouge

The results from our sliding tests on granite demonstrate that frictional strength depends in a complicated manner on several factors: temperature, slip rate, and pore pressure. The mechanical data suggest that sliding behavior can be divided into at least two regimes. The first regime includes dry granite up to at least 845° and wet granite below 250°C. In this regime, samples strain harden, friction is high (0.7 to 0.8), friction depends only modestly on temperature, slip rate, and  $P_{\text{H}_2\text{O}}$ , and the transient response of friction to velocity steps is small and short-lived. To a first order, then, sliding strength in this regime is well-characterized by the relation of *Byerlee* [1978] which relates maximum sliding resistance to effective normal stress. (The relation is  $\tau = 0.85\bar{\sigma}_n$  MPa for  $\bar{\sigma}_n \leq 200$  MPa;  $\tau = 0.6\bar{\sigma}_n + 50$  MPa for  $\bar{\sigma}_n > 200$  MPa. Thus, for  $\bar{\sigma}_n = 400$  MPa,  $\mu = 0.725$ .) The second regime includes wet granite above  $\sim 350^\circ\text{C}$ . In this regime, friction is sensitive to temperature, slip rate, and  $P_{\text{H}_2\text{O}}$ , and strain weakening is observed above  $\sim 350^\circ\text{--}400^\circ\text{C}$ . Maximum sliding resistance in this regime cannot be predicted from *Byerlee's* relation and knowledge of the effective stress.

This interpretation is consistent with the two regimes identified for quartz gouge by *Chester and Higgs* [1992]. They call on a broad, transitional regime, in which brittle, cataclastic flow gives way to a plastic flow mechanism, most likely solution transport creep, with increasing temperature and/or decreasing slip rate. As for granite, friction of quartz deformed at low rates in the hydrothermal regime depends on temperature, slip rate, and  $P_{\text{H}_2\text{O}}$ . Quartz displays significant reduction in strength only at the very low slip rates reached in slide-hold-slide (stress relaxation) tests, however. Our granite experiments present two advantages over *Higgs'* [1981] tests on quartz: First, we have performed tests at more closely spaced temperatures. Second, the velocity dependence of steady state friction is estimated with more confidence from velocity step tests than from numerical modeling of slide-hold-slide relaxations [*Chester and Higgs*, 1992].

The addition of water at high temperature causes weakening at constant effective stress. From this we infer that one or more

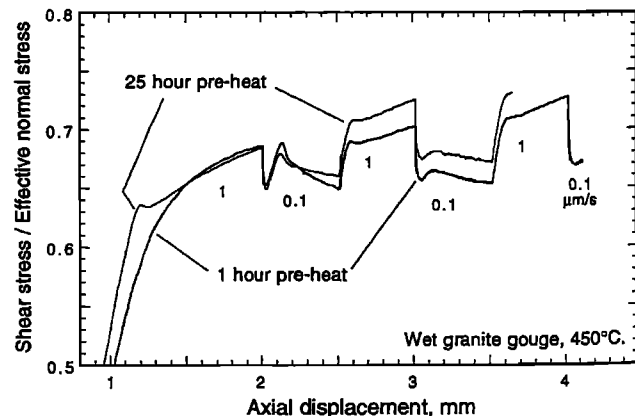


**Figure 9.** Friction displacement curves for granite gouge slid at 450°C with  $\bar{\sigma}_n = 400$  MPa and  $P_{\text{H}_2\text{O}} = 100$  MPa. An additional 24 hours of preheating before deformation causes a small strength peak at the initiation of sliding; however, subsequent slip is nearly unaffected.

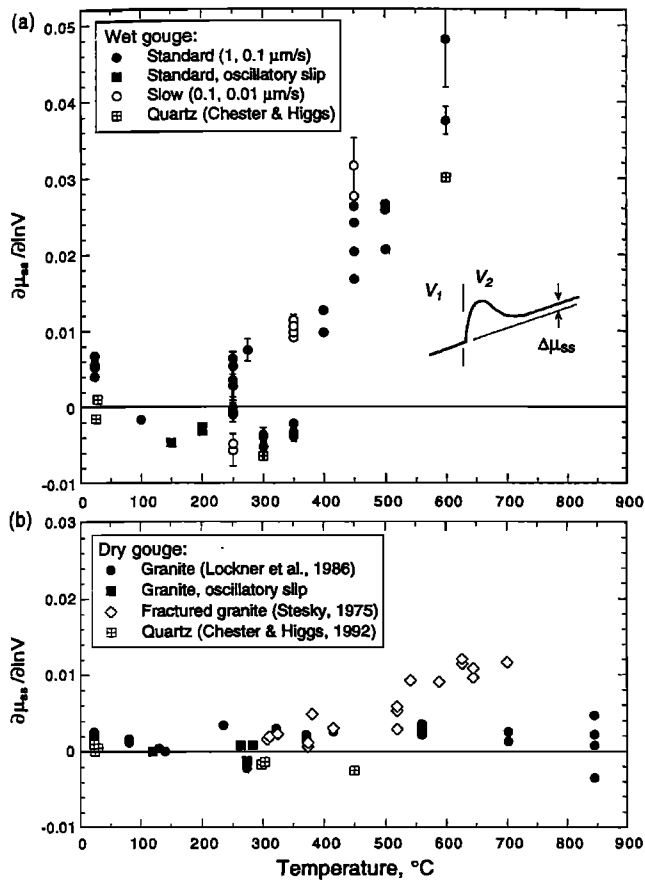


**Figure 10.** Velocity dependence of steady state friction for wet and dry granite and quartz gouges. The inset illustrates how  $\Delta\mu_{ss}$  was estimated for the granite gouge. (a)  $\partial\mu_{ss}/\partial\ln V$  versus temperature for wet granite gouge, plus determinations for wet, ultrafine quartz powder, determined through modeling of stress relaxations by *Chester and Higgs* [1992]. (b) Values for dried granite gouge [*Lockner et al.*, 1986, Figure 7] (for steps between 0.5 and 5.5  $\mu\text{m/s}$  at axial displacements  $\geq 2.5$  mm), prefractured dry granite [*Stesky*, 1975], and dry, ultrafine quartz powder [*Chester and Higgs*, 1992].

fluid-aided deformation processes are activated in the second regime and operate concurrently with cataclastic flow. If this inference is correct, then deformation is best described as transitional between purely brittle and purely plastic flow. Evidence for plastic deformation includes the marked dependencies of strength on temperature and deformation rate. Evidence for brittle deformation includes particle size reduction and a dependence of strength on effective stress. Effective stress dependence was measured by deforming a single gouge sample at 500°C, 1  $\mu\text{m/s}$ ,  $P_{\text{H}_2\text{O}} = 100$  MPa, and confining pressures of 300, 400, and 500 MPa. Residual strength increased monotonically with effective normal stress ( $\partial\tau/\partial\sigma_n \approx 0.43$ ).

Microstructural evidence for the activation of fluid-aided deformation mechanisms may be difficult to recognize. Optical-scale deformation textures in the gouge are dominated by the results of cataclasis, so features indicative of, for instance, solution transport deformation are obscured if present. The extremely fine particle size and mixture of phases in the gouge also complicate analysis. The similarity between the mechanical results for granite and those for quartz gouge [*Higgs*, 1981; *Chester and Higgs*, 1992] suggests that solution transport creep may be activated;

however, we lack direct evidence of this process. For example, *Higgs* observed veins in quartz gouge suggesting transport of dissolved material through the pore fluid, but we not seen them here. Several alternatives exist. Acceleration of subcritical crack growth at higher temperature might allow cataclastic flow to occur at lower stress but might not result in a distinctly different microstructure. Also, feldspar is metastable at the run conditions and may break down to form phyllosilicates or zeolites. However, it is unlikely that a large enough volume of new minerals is produced to affect the bulk strength of the gouge; the starting material contains about 5% biotite and a small amount of muscovite, so the addition of a small additional amount of either is not expected to dramatically lower the strength. Feldspar may undergo incongruent pressure solution, dissolving at load-bearing points of contact and precipitating elsewhere as stable phyllosilicates or zeolites [*Beach*, 1980]. In this case, although the mineralogical reactions would be the same, strength may be influenced by the kinetics of feldspar dissolution, rather than by the strength of the reaction products. Weakening via incongruent pressure solution remains largely unverified in the laboratory [*Rubie*, 1990], although *Pinkston et al.* [1987] correlated weakening in laboratory faults in dunite with the retrograde reaction to serpentine on the sliding surface.

Alternatively, deformation in these experiments may be dominated by the effects of rapid dissolution into an undersaturated pore fluid. It seems possible that rapid dissolution at load-bearing contacts accommodates rapid shearing and compaction. Were this true, then the attainment of an equilibrium saturation state in the pore fluid would cause a recovery of strength. However, the kinetics of dissolution are rapid at the hydrothermal conditions of these experiments. Consider, for example, dissolution of a quartz powder in initially pure  $\text{H}_2\text{O}$ , a problem for which many data exist. For simplicity, we represent the powder as uniform, closely packed, 100- $\mu\text{m}$ -diameter spheres. For dissolution at  $P_{\text{H}_2\text{O}} = 100$  MPa, *Rimstidt and Barnes* [1980] give a time constant of saturation of just 1 hour at 250°C. *Dewers and Hajash* [this issue] dissolved quartz powder of 90–120  $\mu\text{m}$  particle size in water. At 150°C and  $P_{\text{H}_2\text{O}} = 35$  MPa an equilibrium silica saturation was reached in ~55 hours. Using their activation energy for dissolution of 73 kJ/mol (in good agreement with *Rimstidt and Barnes*' 66–76 kJ/mol), we can extrapolate this value to higher temperatures: at 250°C saturation should be achieved, again, in about 1 hour. This number depends on the exact size distribution, angularity, and packing of the powder and will be somewhat different for a granitic composition and for nonzero effective pressure [*Dewers and Hajash*, this issue]. However, most particles in our granite gouge are far smaller than 90  $\mu\text{m}$ , so these calculations should overestimate the time to saturation in our tests. We conclude that fluid saturation was likely achieved prior to shortening in our experiments at temperatures  $\geq 250^\circ\text{C}$ .

### Strain Localization at High Temperatures

The two regimes identified above on the basis of strength and velocity dependence appear to correspond to distinct microstructures. Samples deformed in the first regime (low temperatures and/or dry; high strength) show pervasive shearing of the gouge layer. We infer that the tendency for deformation to remain delocalized results from strain hardening, because maximizing the width of shearing decreases the rate of strain accumulation. Delocalized shearing is accompanied by the formation of numerous  $R_1$  and Y Riedel shears over a wide range of conditions. The formation of Riedel shears should be encouraged by velocity

weakening friction, because slip rate is thereby increased locally; however, Reidel shears were observed to have formed in gouges showing both positive and negative velocity dependence. Riedel shears have a short "lifetime," either because they rapidly strain harden or because they are poorly oriented for continued slip [Byerlee *et al.*, 1978].

Samples deformed in the second regime (high temperatures and  $P_{H_2O}$ ; decreased strength) show shearing localized onto a boundary-parallel shear zone and few Riedel shears elsewhere in the gouge. Clearly, persistent localized slip implies that slip on the boundary shear zone can occur at stresses lower than those required to deform the surroundings. The boundary shear could be weak due to a high concentration of biotite well-aligned for slip on the basal plane [Shea and Kronenberg, 1993; Wintsch *et al.*, this issue]. Indeed, we infer a concentration of biotite in the boundary shear shown in Figure 2e. However, samples deformed in the first regime contained biotite entrained in  $R_1$  and Y Riedel shears yet remained strong.

Alternatively, the boundary shear could be weak because its particle size is small. Rapid reduction in gouge particle size is most efficient for feldspar [Yund *et al.*, 1990] and is most pronounced near the gouge-rock interface [Dieterich, 1981; Marone and Scholz, 1989]. Thus, deformation near the gouge-rock interface will be favored if strength is sensitive to particle size [see Evans and Wong, 1985]. Several deformation processes mentioned above fall into this category: solution transport creep, incongruent pressure solution, and retrograde reaction of feldspars to weaker products. Continued slip near the interface further widens the contrast in particle size compared to the surrounding gouge, and slip will remain localized so long as strength remains below that of the coarser-grained remainder of the gouge.

A possible strategy to distinguish between these two hypotheses would be to perform hydrothermal sliding tests on powders containing quartz and feldspar but lacking micas. Ultrafine quartz powder deforms homogeneously in the hydrothermal regime without the formation of boundary shears [Higgs, 1981]. This contrast to granite gouge may result from the lack of mica, the lack of feldspars to undergo mineral reactions, or the initially fine particle size, which may have prevented the gouge from developing a sufficiently large contrast in particle size to overcome the tendency for homogeneous deformation.

## Rheological Model

To allow prediction of frictional strength at conditions of slip rate and temperature outside those encompassed by our suite of experiments, we fit our measurements of steady state friction with a rate- and temperature-dependent constitutive law proposed by Chester [1988, 1994, this issue]. Chester incorporated temperature into the so-called Dieterich–Ruina constitutive law [Dieterich, 1979; Ruina, 1983] which was built on laboratory observations showing that frictional strength depends both on slip rate and on the recent history of sliding. (These are features which give rise to the transient evolution of strength following velocity steps at constant temperature, Figure 6. See Dieterich [1979].) In adding temperature dependence, Chester retained the rate and history dependence of the earlier law. The reader may refer to Chester [1994] for details on the rationale, development, and preliminary testing of the full formulation. Here, we are concerned only with variations to steady state friction:

$$\mu_{ss} = \mu_* + (a-b) \ln \left( \frac{V}{V_*} \right) + \frac{aQ_a - bQ_b}{R} \left( \frac{1}{T} - \frac{1}{T_*} \right). \quad (2a)$$

The parameter  $a$  scales the "direct effect" (an instantaneous dependence of friction on slip rate), while parameter  $b$  scales the "evolution effect" (the evolution of friction toward a steady state value appropriate for a given slip rate).  $Q_a$  and  $Q_b$  are apparent activation enthalpies associated with the direct ( $a$ ) and evolution ( $b$ ) transient effects, respectively,  $T$  is absolute temperature, and  $R$  is the universal gas constant.  $V_*$ ,  $T_*$ , and  $\mu_*$  are reference parameters such that  $\mu_{ss} = \mu_*$  when  $V = V_*$  and  $T = T_*$ . Parameters  $a$  and  $b$  are generally measured to be a few percent or less of  $\mu_{ss}$ . Thus  $\mu_*$  identifies a nominal friction value, and the subsequent terms give the second-order dependence on slip rate and temperature. We lack sufficient information to distinguish separate activation enthalpies  $Q_a$  and  $Q_b$  for granite and therefore treat them as equal ( $Q_a = Q_b = Q$ ), in which case (2a) reduces to

$$\mu_{ss} = \mu_* + (a-b) \left[ \ln \left( \frac{V}{V_*} \right) + \frac{Q}{R} \left( \frac{1}{T} - \frac{1}{T_*} \right) \right]. \quad (2b)$$

The steady state velocity dependence of friction (at fixed temperature) is

$$\partial \mu_{ss} / \partial \ln V = a-b \quad (3)$$

such that positive values indicate velocity strengthening, and negative values indicate velocity weakening. The steady-state temperature dependence (at fixed slip rate) is most conveniently given in terms of inverse temperature:

$$\frac{\partial \mu_{ss}}{\partial T^{-1}} = \frac{aQ_a - bQ_b}{R} = (a-b) \frac{Q}{R} \quad (4)$$

such that positive values indicate temperature weakening, and negative values temperature strengthening [Chester, 1994].

Chester and Higgs [1992] treated each frictional regime as dominated by a single deformation mechanism and reasoned that deformation within each frictional regime can be represented by the rate- and temperature-dependent law (2). Each regime is described by an independent set of constitutive parameters; it follows from (3) and (4) that within each regime the velocity dependence and temperature dependence of friction are constant. Chester and Higgs obtained parameter values for each of the two regimes for quartz described above. Chester [this issue] further subdivides deformation at lower temperatures into two regimes, although both involve purely brittle deformation. The first of these, operating at the lowest temperatures, is characterized in quartz by distributed grain size reduction and velocity strengthening. The second, operating at intermediate temperatures, is characterized by slip localization and velocity weakening. The deformation microstructures in our granite cannot clearly be differentiated into delocalized and localized slip regimes at low temperatures. However, we do measure a transition from velocity strengthening to velocity weakening at  $\sim 100^\circ\text{C}$  (Figure 10a). Although this transition is gradual rather than abrupt, it is consistent with Chester's interpretation. On this basis we choose to follow the procedure of Chester [this issue] and fit the granite data with three independent sets of constitutive parameters.

We find that the major features of Figures 6 and 10a can be matched with a unique set of constitutive parameters (Figure 11). Table 2 lists the parameter values used to calculate the fit in Figure 11 and, for comparison, those presented by Chester for quartz. Several features of the data set are well-represented by the three-regime fit. These include the overall level of friction, the slight increase of friction with temperature up to  $\sim 300^\circ$  and more pronounced decrease above  $\sim 350^\circ$ , and the velocity dependence

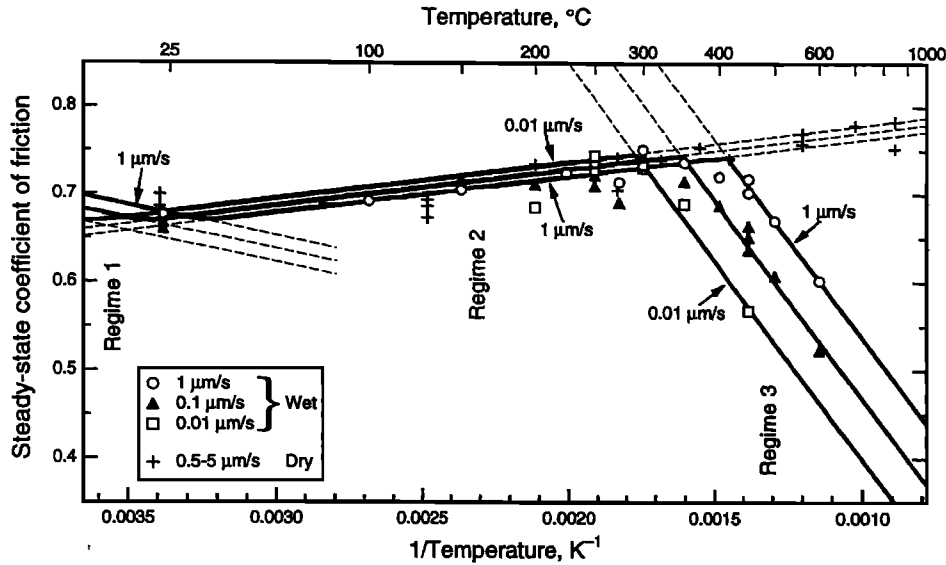


**Figure 11.** Friction of granite gouge (values from Figure 6) fit with a rate- and temperature-dependent law for steady state friction (equation 2). See text and the appendix for explanation of the model. Contours of constant velocity are drawn with dashed lines for three independent sets of model parameters (Table 2). Solid contours show the net predicted strength at slip rates of 1, 0.1, and 0.01  $\mu\text{m/s}$ .

of strength at the highest temperatures. The appendix presents more details about the model fit and the constraints available for the various parameters and compares the model velocity dependence and temperature dependence with the experimental values. M.L. Blanpied et al. [manuscript in preparation, 1995] model the response to velocity steps in both dry and hydrothermal experiments to obtain values for friction constitutive parameters and to evaluate the adequacy of rate and state constitutive laws to describe frictional behavior at hydrothermal conditions.

**Extrapolations to Natural Faults**

Extrapolation of laboratory strength data to crustal conditions is commonly done with reference to plots of maximum strength versus depth [e.g., Goetze and Evans, 1979]. The simplest of these diagrams uses Byerlee’s law to characterize the uppermost, presumably brittle crust, and a power law relation to describe the strength of the deeper crust where deformation by intracrystalline

plasticity is expected [e.g., Brace and Kohlstedt, 1980]. It is commonly recognized that fluid-assisted deformation, as well as superhydrostatic fluid pressures, may reduce the strength of the upper crust to midcrust to levels far below that prescribed by these two-layer models [e.g., Kirby, 1980; Sibson, 1983; Byerlee, 1990, 1993; Rice, 1992; Sleep and Blanpied, 1992, 1994]. However, little quantitative information on the strength of rocks deforming by these means is available to construct quantitative crustal models. For example, Cox and Etheridge [1989] presented evidence for solution precipitation creep accompanying deformation of silicic volcanic rocks during prograde metamorphism. They inferred from an abundance of healed microcracks that deformation occurred at high fluid pressures (approaching lithostatic) and differential stress levels of some tens of megapascals at most and suggested more generally that the midcrustal, high-stress peak predicted by two-layer models is reduced by solution precipitation creep. Janecke and Evans [1988] found that exhumed shear zones in granite were weakened by the muscovite

**Table 2.** Parameters in the Rate- and Temperature-Dependent Constitutive Law for Friction, with Values Determined for Quartz and Granite Gouges

Parameter	Units	Granite (this study)			Quartz [Chester, this issue]		
		Regime 1	Regime 2	Regime 3	Regime 1	Regime 2	Regime 3
$a$		0.0075	0.0075	0.02	0.0062	0.006	0.03
$b$		0.0010	0.0110	-0.01	0.0042	0.011	0
$Q_a$	kJ/mol	89	100	125	89	78	44
$Q_b$	kJ/mol	89	100	125	89	78	—
$\mu_*$		0.678	0.705	0.602	0.638	0.737	0.850
$V_*$	$\mu\text{m/s}$	1	1	1	$\#/1000^a$	1	$\#/1000^a$
$T_*$	K	298	423	873	573	573	573
$\partial\mu_{ss}/\partial\ln V$		+0.0065	-0.0035	+0.03	+0.0020	-0.005	+0.03
$\partial\mu_{ss}/\partial(1/T)$	K	+69	-42	+451	+21.4	-47.4	+159

<sup>a</sup> Chester’s  $V_*$  is scaled by gouge layer thickness  $t$  (in micrometers) for regimes 1 and 3.

produced by retrograde breakdown of feldspar. Their resulting rheological model uses laboratory data for the shearing strength of muscovite to represent midcrustal strengths and is therefore somewhat more quantitative than many other studies. *Kronenberg et al.* [1990] measured the strength of biotite single crystals oriented for easy basal glide. Strength was low and insensitive to normal stress and slip rate. A yield envelope extrapolated to natural conditions predicts a strength of a few tens of megapascals from the Earth's surface to 25 km depth, assuming that slip occurs on well-oriented biotite basal planes. *Chester* [this issue] presents a model, based on analysis of quartz rheology, which includes a midcrustal layer within which deformation occurs by combined cataclasis and solution transport creep. Because our data for granite span a broad range of conditions, they can help to define the characteristics of such an intermediate rheological layer in a granitic crust.

We take three logical steps to extrapolate the laboratory results and fitted constitutive law to natural faults. First, we define a correspondence between the experimental temperature and depth using an appropriate geotherm. Second, we define how the laboratory values of  $\mu$  are to be extrapolated to the natural setting at those depths. Third, we assign conditions of normal stress and pore pressure in order to calculate shear strength from (1). We examine two cases: the first for hydrostatic fluid pressure throughout the crust, the second for superhydrostatic fluid pressure which is elevated to near lithostatic at depth. It is readily apparent that the first case will predict high fault strength at seismogenic depths, as our measurements agree well with Byerlee's law to temperatures as high as  $\sim 350^\circ\text{C}$ . Thus the data do not support the hypothesis that "weak" faulting derives from a low coefficient of friction in the absence of locally elevated fluid pressure (see *Hickman* [1991] for a discussion of weak fault models.)

One additional consideration is the method for extrapolating from laboratory to natural deformation rates. The laboratory data are described in terms of slip rate. If slip is localized onto a surface both in the laboratory and in the field, then it is probably appropriate to extrapolate in terms of slip rate rather than strain rate [cf. *Chester*, this issue]. Evidence of localized slip in the hydrothermal regime supports this approach for the granite data, and it is the one we follow below. The lowest slip rate studied here,  $0.01 \mu\text{m/s} = 315 \text{ mm/yr}$ , is only about 10 times faster than the time-averaged slip rate of the San Andreas fault. Therefore the extrapolation in slip rate from the lab to nature may be done with some confidence. However, if shearing is delocalized, then it is more appropriate to extrapolate in terms of shear strain rate rather than slip rate. For quartz gouge this appears to be the case [*Higgs*, 1981]. This requires the width of both the experimental and natural shear zones to be known [*Chester*, this issue], and the required extrapolations may be to strain rates several orders of magnitude beyond the range of the data set.

We use temperature to assign a correspondence between the experimental conditions and crustal depth. We employ two geotherms calculated from measurements of heat flow and thermal conductivity in the Coast Ranges of California, through which runs the San Andreas [*C. Williams et al.*, unpublished data, 1992]. One geotherm, "A" in Figure 12a, is calculated with the assumption that heat is generated in the upper crust by shearing in the San Andreas fault system (strong fault model). The geothermal gradient decreases with depth, from  $30^\circ\text{C/km}$  at the surface to less than  $20^\circ\text{C/km}$  below 20 km (Figure 12b). The second geotherm, "B", is calculated with the assumption that shear-

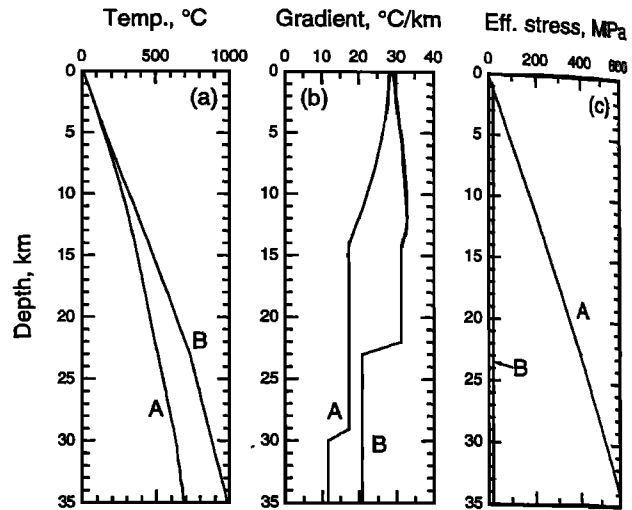


**Figure 12.** Temperature and pore pressure profiles assumed in the extrapolation of experimental friction data to natural fault slip (see Figure 13). (a) Two geotherms calculated for the California Coast Ranges based on near-surface heat flow measurements (*C. Williams et al.*, written communication, 1992). Geotherm A is calculated assuming that slip on the San Andreas fault generates heat in the upper crust. Geotherm B assumes that slip on the San Andreas fault generates no heat. (b) Thermal gradients for geotherms A and B. (c) Effective stress versus depth assumed in two extrapolations. The right-hand line assumes  $\sigma_n = 27.5 \text{ MPa/km}$  and  $P_p = 10 \text{ MPa/km}$  (hydrostatic case). The left-hand line assumes elevated pore pressure in the fault according to the model of *Rice* [1992].

ing on the San Andreas generates no heat (weak fault model), an assumption supported by the lack of a well-defined heat flow peak over the fault and the observation that the maximum horizontal stress is at high angles to the fault [see *Hickman*, 1991]. In the latter case the broad region of generally elevated heat flow in the coast ranges is assumed to result from horizontally dispersed high temperatures in the deep crust, and the geothermal gradient is fairly uniform, about  $30^\circ\text{C/km}$ , to 23 km depth. These two geotherms correspond approximately (and in spirit) to the models, A and B, respectively, of *Lachenbruch and Sass* [1973].

Consider first the case for a strong fault, specifically, a fault deforming by frictional sliding with a pore pressure equal to the hydrostatic gradient. Using geotherm "A",  $600^\circ\text{C}$  (the highest temperature tested in our gouge experiments) corresponds to a depth of 28.5 km (Figure 12a). The coefficient of friction shows a maximum at a depth that depends on the rate of sliding (Figure 13a). This peak marks a transition from velocity weakening and temperature strengthening at shallower depths to velocity strengthening and temperature weakening at greater depths. For a sliding rate of  $0.001 \mu\text{m/s} = 31 \text{ mm/yr}$ , the transition depth is  $\sim 9 \text{ km}$ .

Further simplifying assumptions are needed to construct a strength-depth plot. First, we assume that  $\mu$  is insensitive to  $\sigma_n$ , such that the values of  $\mu$  measured at  $\sigma_n = 400 \text{ MPa}$  may be applied to different effective stresses and that over the entire range of conditions shear strength may be calculated by (1). (The assumption that  $\mu$  is independent of  $\sigma_n$  is not strictly correct for our data at higher temperatures and may lead to systematic errors in extrapolating strength within the hydrothermal regime.) Second,

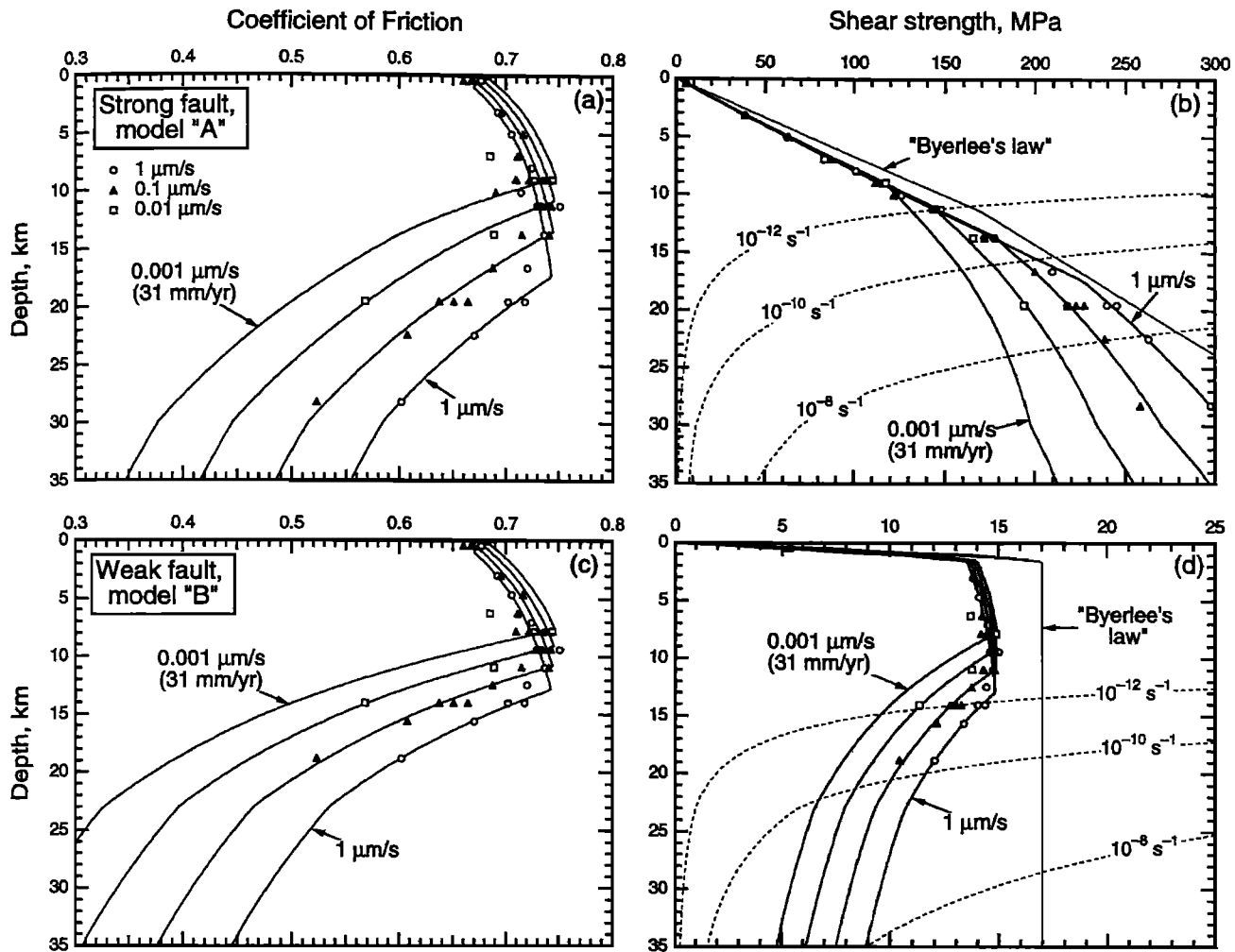


**Figure 13.** Extrapolation of experimental friction data for wet granite gouge to conditions of crustal faulting. (a) Steady state friction values and model fit from Figure 11, extrapolated to depth using geotherm A from Figure 12a. A constant velocity contour at  $0.001 \mu\text{m/s} = 31 \text{ mm/yr}$  is also shown. (b) Shear strength versus depth calculated by multiplying the coefficient of friction from Figure 13a by effective normal stress from Figure 12c (hydrostatic pore pressure case). "Byerlee's law" [Byerlee, 1978] is shown for reference, along with contours of equal strain rate  $\dot{\gamma}$  as predicted by a power law fit for semibrittle flow of wet granite [Hansen and Carter, 1982]. The contour at  $\dot{\gamma} = 10^{-10}/\text{s}$  corresponds to a slip rate of 31 mm/yr distributed over a fault 10 meters wide. (c) Coefficient of friction extrapolated to depth using geotherm B. (d) Shear strength versus depth calculated by multiplying coefficient of friction from Figure 13c by effective normal stress from Figure 12c (overpressured fault case). Note change in scale: calculated strength does not exceed 16 MPa at any depth.

we assume that effective normal stress equals an overburden stress of 27.5 MPa/km, minus pore pressure with an approximately hydrostatic gradient of 10 MPa/km (Figure 12c). This results in the strengths shown in Figure 13b. Strength at shallow depths corresponds closely to that predicted from room temperature friction data, as expected, while strength deviates to much lower values below the rate-dependent transition depth. Note that calculated strength increases monotonically with depth for the range of slip rates explored here, despite the peak in coefficient of friction. For comparison, we include strength predicted by the relation of Byerlee [1978] and strength at three strain rates predicted by a power law fit for plastic flow of wet granite [Hansen and Carter, 1982]. The latter contours should be viewed with some caution: Hansen and Carter's samples deformed by

"semibrittle flow," a combination of brittle cracking and intracrystalline plasticity, and the use of a power law to extrapolate data for semibrittle flow may not be justified in that it ignores a likely pressure sensitivity.

Somewhat different results are obtained by assuming that fluid pressure is elevated in the fault zone. Extrapolating coefficient of friction to depth using geotherm "B," appropriate for a weak fault, raises the transition depth compared to the earlier example and makes the transition depth less sensitive to slip rate (Figure 13c). The distribution of pore pressure in fault zones is a topic of much recent interest. We select for illustration the pore pressure distribution calculated by Rice [1992]. In Rice's model, elevated pore pressure in the fault zone results from a source of high-pressure fluid at depth, low permeability in the fault zone and sur-

rounding rock, and an exponential dependence of permeability on effective normal stress,  $k = k_0 \exp\{-\bar{\sigma}/\sigma_*\}$ , where  $\sigma_*$  is a constant. Rice's model predicts an increase in effective stress with depth to some shallow depth, below which effective stress is constant. For a choice of model parameters  $k_0 = 20$  MPa and  $\sigma_* = 5$  MPa, the model predicts constant  $\bar{\sigma}_n = 20$  MPa below about 2 km [Rice, 1992, Figure 1.6] (Figure 12c). Using this pore pressure distribution, predicted stresses are low, and change only gradually with depth below 2 km (Figure 13d). Strength rises only slightly to a maximum at the transition depth, with greater depths characterized by falling strength and velocity strengthening friction. The strength distribution in Figure 13d is consistent with the limits on shear stress on the San Andreas fault of ~20 MPa over the depth range 0 to 15 km imposed by the heat flow constraint [Lachenbruch and Sass, 1980, 1992].

In both of these cases, the transition depth from velocity weakening to velocity strengthening (i.e., the inflection points in Figures 13a and 13c) at low slip rates is predicted to depend strongly on slip rate. For a slip rate equal to the average, long-term rate of the San Andreas fault (~31 mm/yr = 0.001  $\mu\text{m/s}$ ), the predicted transition depth is 8 to 9 km (245°C), several kilometers shallower than the seismic–aseismic transition depth of 12 to 15 km observed for portions of the San Andreas fault system. From estimates of temperatures at depth in several geologic environments with a wide range of geothermal gradients, the base of seismicity appears to fall consistently in the range 400° to 450°C [C. Williams, personal communication, 1994]. This correlation appears to hold both near the San Andreas fault zone and in other geologic environments in the western United States.

This discrepancy between model and observation would appear to cast doubts on the applicability of the granite velocity dependence data to faulting behavior at depth. However, several comments are warranted. First, note that the transition depth in the rheological model is a strongly increasing function of slip rate (Figure 13). Therefore it is conceivable that accelerating slip near the base of the seismogenic zone could lower the transition depth sufficiently to allow unstable slip at greater depths while remaining in agreement with the granite data. The model of Li and Rice [1987], for example, predicts accelerating slip due to asthenospheric loading between great earthquakes. Second, the effective stress assumed in Figure 13d lies far below that in our experiments. It is possible that the velocity dependence of friction is different at low effective stress; data are not currently available to evaluate this possibility. Third, and perhaps most important, the rheological model (Figures 11–13) is constructed from laboratory measurements for “steady state” sliding. The strength of a stationary fault may differ considerably from the model. The peak strength, that resisting the initiation of slip on the fault, may increase with time due to asperity welding, crack healing, or compaction creep, as seen in the quartz powder experiments of Fredrich and Evans [1992] discussed above, and in our experiments subjected to long preheat times at high temperature (Figure 8). Conversely, strength of an undrained fault may decrease with time due to time-dependent compaction which raises pore fluid pressure, as seen in the self-sealed tests described by Blanpied *et al.* [1992]. Sleep and Blanpied [1992, 1994] and Sleep [this issue] describe a model for an earthquake cycle on a fault zone partially sealed from its surroundings; interseismic shear creep leads to compaction that elevates fluid pressure, allowing frictional failure at relatively low shear stress. Even in the absence of time-dependent compaction creep, accumulating tectonic stress can cause

changes in fluid pressure through poroelastic effects [Sibson, 1991].

### Concluding Remarks

We have demonstrated that at elevated temperature and elevated  $P_{\text{H}_2\text{O}}$ , granite friction depends on several factors including temperature, slip rate,  $P_{\text{H}_2\text{O}}$ , and (to a limited extent)  $\bar{\sigma}_n$ . This result suggests that fluid-assisted mechanisms may cause weakening of rocks at lower temperatures and far higher deformation rates than expected for intracrystalline plasticity in quartz or feldspar. We have argued that deformation in this regime represents a transition between fully brittle and fully plastic deformation. Because of this complexity, it is difficult to extrapolate the laboratory results to conditions not encompassed by the data set. Additional difficulties arise because of the paucity of flow laws for mixed-mechanism deformation and for multiphase aggregates, from poor knowledge of in situ fluid pressures, fluid chemistries and mineralogies, from uncertainties in the degree of shear localization at depth, and because it is unclear whether to extrapolate in terms of slip rate or strain rate. Nonetheless, even the crude extrapolations presented here suggest that above ~300°C (depths > ~9 km) the strength of slipping faults may be considerably below that inferred from room temperature friction data [e.g., Brace and Kohlstedt, 1980], even at slip rates higher than the San Andreas long-term rate.

Of course, because our results were obtained for laboratory faults in granite, they are probably most directly applicable to natural faults in granitic host rocks. We would not necessarily assume, for example, that the behavior of granite powder matches that of a natural fault gouge rich in clay minerals. Therefore the extrapolations shown in Figure 13 should be considered more illustrative than conclusive. On the other hand, the close correspondence between our results for granite and those for quartz suggests that the data may be of general import to faults in quartzose and quartzofeldspathic rocks under certain crustal conditions. Several additional factors, not explicitly considered in the experiments presented here, are known or suspected to influence deformation by processes such as pressure solution, incongruent pressure solution, and production of weak hydrothermal reaction products. For example, the rates of these processes will likely vary with the pH, ionic concentration, and CO<sub>2</sub> content in pore fluids and with the reactivity of gouge minerals. Fault slip to large displacements can produce extremely fine-grained gouge [Yund *et al.*, 1990], which should accelerate reaction rates. The accumulation of phyllosilicates as hydrothermal reaction products should weaken a fault in two ways: first, by allowing deformation by dislocation glide on basal planes [Wintsch *et al.*, this issue]; and second, by providing high-diffusivity pathways which increase the rate of pressure solution creep [Hickman and Evans, this issue]. Finally, the quartz gouge experiments described earlier demonstrate that shearing at hydrothermal conditions may occur by distributed flow in some circumstances. In that case, laboratory friction data are more properly extrapolated in terms of strain rate than slip rate [Chester, this issue], and extrapolation over many orders of magnitude in strain rate may be required to predict the rheology of a broad, creeping fault zone.

The analysis of quartz frictional rheology by Chester and Higgs [1992] suggests that a well-defined transition temperature separates the cool and hot deformation regimes in the presence of aqueous pore fluid and also that this transition temperature is sensitive to slip rate. Our fit of granite strength data with the tem-

perature-dependent constitutive law (Figure 11) suggests that this transition temperature changes by roughly 50°C per decade change in slip rate. However, this value depends strongly on a loosely constrained choice of parameter values, which reduces confidence that it can be extrapolated far from the experimental conditions. Also, as noted earlier, the granite data support a gradual rather than abrupt transition. These and other complexities shown by the granite frictional behavior call for continued efforts to develop improved constitutive laws to describe and predict frictional rheology over a broad range of conditions.

The experiments described here are exploratory in nature but point to several areas in which more detailed investigation would be useful. Experiments are needed to explore the effects of mineralogy and fluid chemistry on sliding strength at elevated temperatures. Sliding tests combined with optical and TEM-scale observations of the run products are needed to define the mechanisms controlling deformation in the hydrothermal regime. Slide-hold-slide tests at hydrothermal conditions can help to quantify the time-dependent strengthening seen in the quartz experiments of Higgs [1981] and Fredrich and Evans [1992]. Finally, sliding tests to large displacements (centimeters or greater) would help to differentiate "steady state" strength from transient effects due to evolving fluid chemistry and rapid gouge volume change during the first few millimeters of slip. Such long-displacement tests, however, will require an advance of laboratory capabilities beyond those currently available.

It is tempting to invoke fluid-assisted deformation mechanisms to explain the apparently low strength of some major faults such as the San Andreas. However, one must note that fault slip accommodated by a mechanism such as solution precipitation creep implies a large and positive dependence of strength on shearing rate (velocity strengthening), and stick-slip sliding may be precluded. It would therefore appear difficult to invoke these mechanisms to weaken the seismogenic portions of faults. It is possible, however, that inhomogeneity of rock type or gouge particle size over the fault plane allows a portion of the fault to creep at low stress, thereby transferring load to locked fault patches that act as seismic sources. Alternatively, the hydrothermal regime identified in the granite data may correspond to a rheological layer of fault creep at depths below the seismic-aseismic transition. Shearing in this aseismic layer may occur at low shear stress, even at strain rates too high to allow dislocation creep to be the dominant deformation mechanism.

### Appendix: Granite Strength Data Fit With Three-Regime Rheological Model

This appendix explains how we obtained the model fit shown in Figure 11. The model fit captures many features of the strength data for wet granite gouge. However, the fit is poorly constrained by the available data for three reasons. First, the formulation requires that fixed parameter values be chosen to represent behavior over broad ranges of temperature, and these ranges are not clearly delineated by the data. Second, temperature-dependent changes in  $\mu_{ss}$  within each of the three regimes come from the last term in (2) rather than from changes in value of the parameters, yet we have no independent measure of the apparent activation enthalpies  $Q_a$  and  $Q_b$  from our sliding tests (Chester [1994] measured  $\partial\mu_{ss}/\partial(1/T)$  in temperature-stepping sliding tests and obtained  $Q_a$  and  $Q_b$  by modeling the transient response using the assumed constitutive law). Third, the constants  $V_*$ ,  $T_*$ , and  $\tau_*$  may be freely adjusted. Therefore the fit presented here should be

considered as an example only. Other, equally good fits might be obtained with somewhat different parameter values, and we have not attempted to define a criterion to evaluate goodness of fit. Nonetheless, some constraints are available. The following observations were used to obtain the parameters for granite (Table 2).

In the first, coolest regime,  $a-b = 0.0065$  and  $a = 0.0075$  are representative of values obtained from modeling the transient friction response in standard runs at room temperature (M.L. Blanpied et al., manuscript in preparation, 1995).  $Q$  ( $= Q_a = Q_b$ ) is poorly defined by the granite data at low temperature, and we adopt the value of 89 kJ/mol obtained by Chester [1994] from temperature-stepping tests on wet quartz gouge at <100°C. The starred constants ( $V_*$ ,  $T_*$ ,  $\tau_*$ ) were set by requiring the fit to pass through the datum at 23°, 1  $\mu\text{m/s}$ .

In the second, intermediate regime,  $a-b = -0.0025$  and  $a = 0.0075$  were chosen by eye from Figure 10a and the data of M.L. Blanpied et al. (manuscript in preparation, 1995) as representative for the temperature interval 150° to 225°C over which granite showed velocity weakening and small strength transients.  $\partial\mu_{ss}/\partial(T^{-1})$  was obtained from least squares regression of dry strength data from 23° to 845°C and wet data from 23° to 300°C, noting that the strength of dry and wet granite is similar up to at least 300°. This gave  $Q \approx 100$  kJ/mol. The fit was made to pass through the datum at 150°, 1  $\mu\text{m/s}$ .

In the third, highest-temperature regime,  $a-b = 0.03$  was constrained by the six measurements at 450°C (Figure 11a). The individual parameters  $a$  and  $b$  are poorly constrained. The value of  $a = 0.02$  is in the low range of values obtained by modeling of standard runs at and above 400°C. The resulting value of  $b = a - (a-b) = -0.1$  adequately represents the net magnitude of the evolution effect; however, the evolution effect in this regime is actually quite complex (Figure 3c) and requires modeling with a two-state-variable constitutive law (M.L. Blanpied et al., manuscript in preparation, 1995). Temperature dependence  $\partial\mu_{ss}/\partial(T^{-1})$  was constrained by the data at >400°C at 0.1  $\mu\text{m/s}$  and >450°C at 1  $\mu\text{m/s}$  (Figure 11a), giving  $Q = 125$  kJ/mol. However, Stesky [1975] reported  $Q = 100$  kJ/mol for sliding of dry granite from 300° to 500°C and  $Q = 130$  kJ/mol from 500° to 700°C, in good agreement with values chosen here for the second and third regimes, respectively.

To combine the three regimes, we follow the assumptions of Chester [this issue]: First, the deformation processes active in regimes 1 and 2 operate in a series-sequential fashion, such that the process giving rise to the highest resistance is dominant. Second, the deformation processes active in regimes 2 and 3 operate in a parallel-concurrent fashion, such that the process giving rise to the lowest resistance dominates. The behavior of the three-regime model is poorly defined at the temperature/slip rate conditions at which the three regimes meet, so we simply represent the overall behavior as that of the dominant process (heavy lines in Figure 11).

Features of the data set well-represented by the three-regime fit include the overall level of friction, the slight increase of friction with temperature up to ~300° and more pronounced decrease above ~350°C, and the velocity dependence of strength at the highest temperatures (Figure 11a). The nominal strength of dry granite gouge is well matched by the intermediate regime, although dry gouge shows slightly positive velocity dependence above 200°C, not velocity weakening. (Note that when  $Q_a = Q_b$  and  $a$  and  $b$  are positive,  $\partial\mu_{ss}/\partial\ln V$  and  $\partial\mu_{ss}/\partial(T^{-1})$  are of oppo-

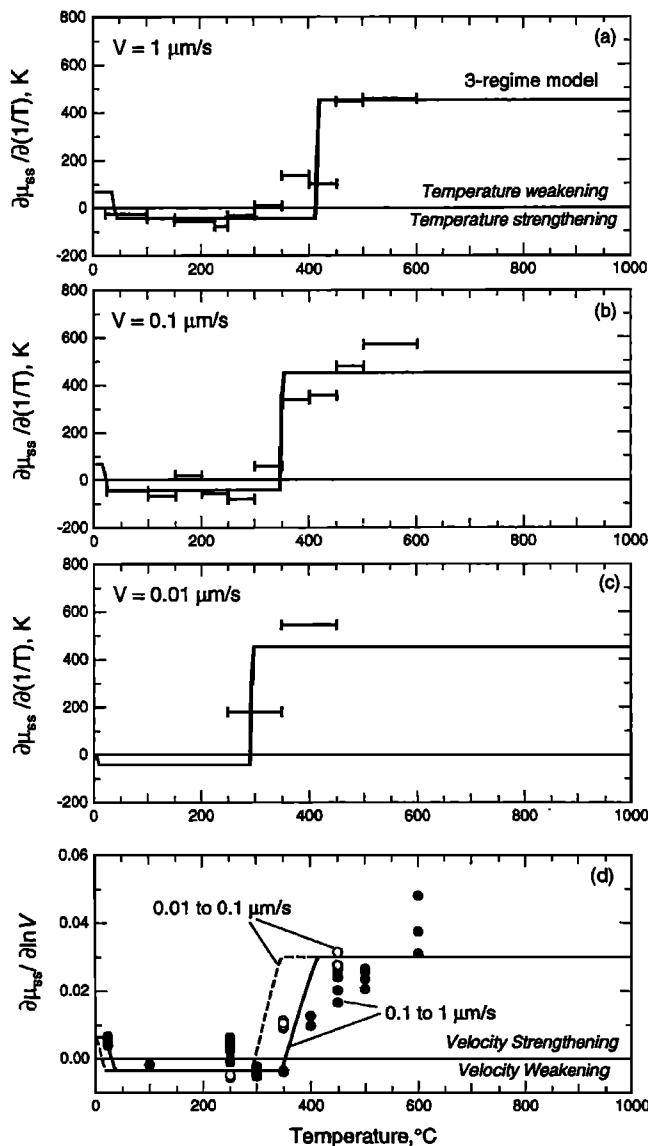


**Figure A1.** Measurements of velocity dependence and temperature dependence of friction for wet granite, with model fit. (a), (b), (c) Temperature dependence of steady state friction for wet granite gouge at  $V = 1$ ,  $0.1$ , and  $0.01 \mu\text{m/s}$ , respectively, calculated over the temperature intervals shown by the horizontal bars and temperature dependence predicted by the fit shown in Figure 11. (d) Velocity dependence of steady state friction for wet granite gouge and temperature dependence predicted by the fit.

site sign, whereas both are positive for dry gouge.) The temperature dependence of friction from the model is compared to the data in Figures A1a–A1c. The model predicts that the transition from temperature strengthening to temperature weakening will decrease by roughly  $50^\circ\text{C}$  per decade decrease in slip rate, in good agreement with the granite data. The model also captures some of the complexity of the velocity dependence data (Figure A1d) including a switch in the sign of  $\partial\mu_{ss}/\partial\ln V$  at  $-100^\circ$  and another at  $250^\circ$ – $350^\circ\text{C}$ .

Figure A2 compares the model fit for granite with Chester's fit for quartz (assuming a shear zone width of  $400 \mu\text{m}$ , Table 2). Contours are drawn for slip rates of  $1 \mu\text{m/s}$  and  $0.001 \mu\text{m/s}$  ( $\approx 31 \text{ mm/yr}$ ). The models match closely at lower temperatures (regimes 1 and 2). In regime 3 the temperature dependence of

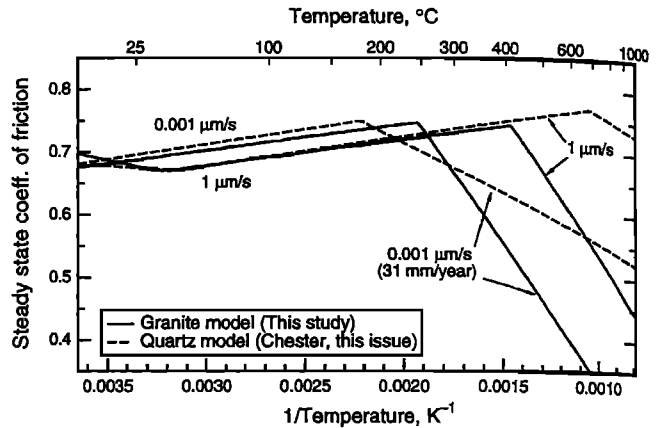


**Figure A2.** Steady state coefficient of friction as a function of temperature predicted by the model fit to granite data from Figure 11 and that predicted by the fit to quartz by Chester [this issue] (Table 2). In the latter case, a gouge thickness of  $400 \mu\text{m}$  was used to calculate the value of  $V_*$ . Contours are drawn for slip rates of  $1 \mu\text{m/s}$  and  $0.001 \mu\text{m/s}$  ( $\approx 31 \text{ mm/yr}$ ). The models for granite and quartz are quite similar, the main difference being the magnitude of temperature weakening in the high-temperature regime.

friction for granite is almost 3 times that for quartz. The temperature of the boundary between regimes 2 and 3 differs markedly at both slip rates. We consider the correspondence between the two models to be close, given that the model for quartz is based on relatively few experimental data and that we lack direct determinations of  $Q_a$  and  $Q_b$  for either rock type.

The model is, by its nature, unable to match several important details. First, the model requires parameter values, and therefore  $\partial\mu_{ss}/\partial\ln V$  and  $\partial\mu/\partial(T^{-1})$ , to be fixed over broad ranges of conditions, whereas the data are not so well behaved. For example, the velocity dependence data are not constant even over small temperature intervals (Figure A1d). Second, the model predicts fairly abrupt transitions in  $\partial\mu_{ss}/\partial\ln V$  and  $\partial\mu/\partial(T^{-1})$ , whereas the velocity dependence data in particular show neither the abrupt transition from small to large velocity dependence nor the constant value at high temperatures, predicted by the model. Rather, the data imply a gradual transition spanning a broad range of temperatures. Possibly, this reflects the complex mixture of phases in the granite. Data for single-phase rocks might be used to test this possibility; however, the existing data for quartz are sparse [Chester and Higgs, 1992] and cannot be used to distinguish between abrupt and gradual boundaries between regimes. Finally, granite shows continued evidence for complex history dependence even at  $600^\circ\text{C}$  in wet tests at  $1$  and  $0.1 \mu\text{m/s}$ , reflected in the oscillatory approach to steady state following velocity steps. Modeling of this behavior requires two state variables (M.L. Blanpied et al., manuscript in preparation, 1995). Therefore a law capable of fully representing the granite behavior would require additional complexity in the hydrothermal regime. It is clear that as additional data on hydrothermal friction becomes available, we can look forward to further developments in temperature-dependent friction constitutive relations.

**Acknowledgments.** This work benefited from interactions with many colleagues. The authors especially thank D. Bartz and R. Summers for assistance in the laboratory; F. Chester, B. Evans, S. Hickman, C. Marone, D. Moore, N. Sleep and T.-f. Wong for valuable discussions; J. Fredrich, B. Hacker, S. Hickman, W. Stuart and J. Weeks for thorough reviews; F.

Chester and C. Williams for providing manuscripts and geotherms, respectively, prior to publication. We also thank S. Hickman, R. Bruhn and R. Sibson for organizing a stimulating workshop and editing this special section of JGR. Research funding was provided by the USGS programs in Earthquake Hazard Reduction and Deep Continental Studies.

## References

- Beach, A., Retrogressive metamorphic processes in shear zones with special reference to the Lewisian complex, *J. Struct. Geol.*, **2**, 257-263, 1980.
- Beeler, N. M., and T. E. Tullis, Implications of Coulomb plasticity for the velocity dependence of experimental faults, *Pure Appl. Geophys.*, in press, 1995.
- Ben-Zion, Y., and J. R. Rice, Slip patterns and earthquake populations along different classes of faults in elastic solids, *J. Geophys. Res.*, this issue.
- Biegel, R. L., C. G. Sammis, and J. H. Dieterich, The frictional properties of simulated gouge having a fractal particle distribution, *J. Struct. Geol.*, **11**, 827-846, 1989.
- Bird, P., Hydration-phase diagrams and friction of montmorillonite under laboratory and geologic conditions, with implications for shale compaction, slope stability, and strength of fault gouge, *Tectonophysics*, **107**, 235-260, 1984.
- Blanpied, M. L., D. A. Lockner, and J. D. Byerlee, Fault stability inferred from granite sliding experiments at hydrothermal conditions, *Geophys. Res. Lett.*, **18**, 609-612, 1991.
- Blanpied, M. L., D. A. Lockner, and J. D. Byerlee, An earthquake mechanism based on rapid sealing of faults, *Nature*, **358**, 574-576, 1992.
- Brace, W. F., and D. L. Kohlstedt, Limits on lithospheric stress imposed by laboratory experiments, *J. Geophys. Res.*, **85**, 6248-6252, 1980.
- Byerlee, J., Friction of rocks, *Pure Appl. Geophys.*, **116**, 615-626, 1978.
- Byerlee, J., Friction, overpressure and fault normal compression, *Geophys. Res. Lett.*, **17**, 2109-2112, 1990.
- Byerlee, J., Model for episodic flow of high pressure water in fault zones before earthquakes, *Geology*, **21**, 303-306, 1993.
- Byerlee, J. D., and J. C. Savage, Coulomb plasticity within the fault zone, *Geophys. Res. Lett.*, **19**, 2341-2344, 1992.
- Byerlee, J. D., V. Mjachkin, R. Summers, and O. Voevoda, Structures developed in fault gouge during stable sliding and stick-slip, *Tectonophysics*, **44**, 161-171, 1978.
- Chester, F. M., Temperature and rate dependence of friction for faults (abstract), *Eos Trans. AGU*, **69**, 471, 1988.
- Chester, F. M., Effects of temperature on friction: Constitutive equations and experiments with quartz gouge, *J. Geophys. Res.*, **99**, 7247-7262, 1994.
- Chester, F. M., A rheologic model for wet crust applied to strike-slip faults, *J. Geophys. Res.*, this issue.
- Chester, F. M. and N. G. Higgs, Multimechanism friction constitutive model for ultrafine quartz gouge at hypocentral conditions, *J. Geophys. Res.*, **97**, 1859-1870, 1992.
- Cox, S. F., and M. A. Etheridge, Coupled grain-scale dilatancy and mass transfer during deformation at high fluid pressures: Examples from Mount Lyell, Tasmania, *J. Struct. Geol.*, **11**, 147-162, 1989.
- Dewers, T., and A. Hajash, Rate laws for water-assisted compaction and stress-induced water-rock interaction in sandstones, *J. Geophys. Res.*, this issue.
- Dieterich, J. D., Time-dependent friction and the mechanics of stick-slip, *Pure Appl. Geophys.*, **116**, 790-806, 1978.
- Dieterich, J. D., Modeling of rock friction, 1, Experimental results and constitutive equations, *J. Geophys. Res.*, **84**, 2161-2168, 1979.
- Dieterich, J. D., Constitutive properties of faults with simulated gouge, in *Mechanical Behavior of Crustal Rocks, The Handin Volume*, *Geophys. Monogr. Ser.*, vol. 24, edited by N. L. Carter, M. Friedman, J. M. Logan, and D. W. Stearns, pp. 103-120, AGU, Washington, D.C., 1981.
- Dieterich, J. H., A model for the nucleation of earthquake slip, in *Earthquake Source Mechanics*, *Geophys. Monogr. Ser.*, vol. 37, edited by S. Das, J. Boatwright and C. H. Scholz, pp. 37-47, AGU, Washington, D.C., 1986.
- Dieterich, J. H., Earthquake nucleation on faults with rate- and state-dependent strength, *Tectonophysics*, **211**, 115-134, 1992.
- Dieterich, J. H., and M. F. Linker, Fault stability under conditions of variable normal stress, *Geophys. Res. Lett.*, **19**, 1691-1694, 1992.
- Evans, B. and T.-F. Wong, Shear localization in rocks induced by tectonic deformation, in *Mechanics of Geomaterials*, edited by Z. Bazant, pp. 189-210, John Wiley, New York, 1985.
- Fredrich, J. and B. Evans, Strength recovery along simulated faults by solution transfer processes, in *Proc. U.S. Symp. on Rock Mech.*, **33rd**, pp. 121-130, 1992.
- Goetze, C., and B. Evans, Stress and temperature in the bending lithosphere as constrained by experimental rock mechanics, *Geophys. J. R. Astron. Soc.*, **59**, 463-478, 1979.
- Hansen, F. D. and N. L. Carter, Creep of selected crustal rocks at 1000 MPa (abstract), *EOS, Trans. AGU*, **63**, 437, 1982.
- Hickman, S. H., Stress in the lithosphere and the strength of active faults, *U.S. Natl. Rep. Int. Union of Geod. Geophys. 1987-1990*, *Rev. Geophys.*, **29**, 759-775, 1991.
- Hickman, S. H., and B. Evans, The kinetics of pressure solution at halite-silica interfaces and intergranular clay films, *J. Geophys. Res.*, this issue.
- Higgs, N. G., *Mechanical properties of ultrafine quartz, chlorite and bentonite in environments appropriate to upper-crustal earthquakes*, Ph.D. dissertation, 267 pp., Tex. A & M, College Station, 1981.
- Janecke, S. U., and J. P. Evans, Feldspar-influenced rock rheologies, *Geology*, **16**, 1064-1067, 1988.
- Kilgore, B. D., M. L. Blanpied, and J. H. Dieterich, Velocity dependent friction of granite over a wide range of conditions, *Geophys. Res. Lett.*, **20**, 903-906, 1993.
- Kirby, S. H., Tectonic stresses in the lithosphere: Constraints provided by the experimental deformation of rocks, *J. Geophys. Res.*, **85**, 6353-6363, 1980.
- Kronenberg, A. K., S. H. Kirby, and J. Pinkston, Basal slip and mechanical anisotropy of biotite, *J. Geophys. Res.*, **95**, 19,257-19,278, 1990.
- Lachenbruch, A. H. and J. H. Sass, Thermomechanical aspects of the San Andreas fault system, in *Proceedings of Conference on Tectonic Problems San Andreas Fault System*, edited by A. Nur and R. Kovach, 192-205, Stanford University, Stanford, Calif., 1973.
- Lachenbruch, A. H., and J. H. Sass, Heat flow and energetics of the San Andreas fault zone, *J. Geophys. Res.*, **85**, 6185-6223, 1980.
- Lachenbruch, A. H., and J. H. Sass, Heat flow from Cahon Pass, fault strength, and tectonic implications, *J. Geophys. Res.*, **97**, 4995-5015, 1992.
- Li, V. C., and J. R. Rice, Crustal deformation in great California earthquake cycles, *J. Geophys. Res.*, **92**, 11533-11551, 1987.
- Linker, M., and J. Dieterich, Effects of variable normal stress on rock friction: Observations and constitutive equations, *J. Geophys. Res.*, **97**, 4923-4940, 1992.
- Lockner, D. A., and J. D. Byerlee, Laboratory measurements of velocity-dependent frictional strength, *U.S. Geol. Surv. Open File Rep.*, **86-417**, 1986.
- Lockner, D. A., and J. D. Byerlee, How geometric constraints contribute to the weakness of mature faults, *Nature*, **363**, 250-252, 1993.
- Lockner, D. A., and J. D. Byerlee, Dilatancy in hydraulically isolated faults and the suppression of instability, *Geophys. Res. Lett.*, **21**, 2353-2356, 1994.
- Lockner, D. A., and B. Evans, Densification of quartz powder and reduction of conductivity at 700°C, *J. Geophys. Res.*, this issue.
- Lockner, D. A., R. Summers, and J. D. Byerlee, Effects of temperature and sliding rate on frictional strength of granite, *Pure Appl. Geophys.*, **124**, 445-469, 1986.
- Logan, J. M., M. Friedman, N. Higgs, C. Dengo, and T. Shimamoto, Experimental studies of simulated gouge and their application to studies of natural fault zones, in *Proceedings of Conference VIII, Analysis of Actual Fault Zones in Bedrock*, *U.S. Geol. Surv. Open File Rep.*, **79-1239**, 305-343, 1970.
- Marone, C., and C. H. Scholz, Particle-size distribution and microstructures within simulated fault gouge, *J. Struct. Geol.*, **11**, 799-814, 1989.
- Marone, C., C. B. Raleigh, and C. H. Scholz, Frictional behavior and constitutive modeling of simulated fault gouge, *J. Geophys. Res.*, **95**, 7007-7025, 1990.
- Moore, D. E., R. Summers, and J. D. Byerlee, Strength measurements of heated illite gouge at low and high pore pressures, *U.S. Geol. Surv. Open File Rep.*, **86-578**, 28 pp., 1986a.
- Moore, D. E., R. Summers, and J. D. Byerlee, The effects of sliding velocity on the frictional and physical properties of heated fault gouge, *Pure Appl. Geophys.*, **124**, 31-52, 1986b.
- Morrow, C. A., and J. D. Byerlee, Experimental studies of compaction and dilatancy during frictional sliding on faults containing gouge, *J. Struct. Geol.*, **11**, 815-825, 1989.
- Morrow, C., B. Radney, and J. Byerlee, Frictional strength and the effec-

- tive pressure law of montmorillonite and illite clays, in *Fault Mechanics and Transport Properties in Rocks (the Brace Volume)*, edited by B. Evans and T.-F. Wong, pp. 69-88, Academic, San Diego, Calif., 1992.
- Pinkston, J., L. Stern, and S. Kirby, Hydrothermal reactions on artificial fault surfaces in dunite: fibrous mineral growth, slickensides and temperature sensitivity of reaction weakening, *Eos Trans. AGU*, **68**, 405, 1987.
- Power, W. L., and T. E. Tullis, The relationship between slickenside surfaces in fine-grained quartz and the seismic cycle, *J. Struct. Geol.*, **11**, 879-893, 1991.
- Reinen, L. A., J. D. Weeks, and T. E. Tullis, The frictional behavior of serpentinite: Implications for aseismic creep on shallow crustal faults, *Geophys. Res. Lett.*, **18**, 1921-1924, 1991.
- Reinen, L. A., J. D. Weeks, and T. E. Tullis, The frictional behavior of lizardite and antigorite serpentinites: Experiments, constitutive models, and implications for natural faults, *Pure Appl. Geophys.*, **143**, 317-358, 1994.
- Rice, J. R., Fault stress states, pore pressure distributions, and the weakness of the San Andreas Fault, in *Fault Mechanics and Transport Properties in Rocks (the Brace Volume)*, edited by B. Evans and T.-F. Wong, pp. 475-503, Academic, San Diego, Calif., 1992.
- Rice, J. R., Spatio-temporal complexity of slip on a fault, *J. Geophys. Res.*, **98**, 9885-9908, 1993.
- Rice, J. R., and A. L. Ruina, Stability of steady frictional slipping, *J. Appl. Mech.*, **105**, 343-349, 1983.
- Rimstidt, J. D., and H. L. Barnes, The kinetics of silica-water reactions, *Geochem. Cosmochim. Acta*, **44**, 1683-1699, 1980.
- Rubie, D. C., Mechanisms of reaction-enhanced deformability in minerals and rocks, in *Deformation Processes in Minerals, Ceramics and Rocks*, edited by D. J. Barber and P. G. Meredith, pp. 262-295, Unwin Hyman, Boston, Mass., 1990.
- Ruina, A. L., Friction laws and instabilities: A quasi-static analysis of some dry frictional behavior, Ph.D. dissertation, Brown Univ., Providence, RI, 1980.
- Ruina, A. L., Slip instability and state variable friction laws, *J. Geophys. Res.*, **88**, 10359-10370, 1983.
- Rutter, E. H., Pressure solution in nature, theory and experiment, *J. Geol. Soc. London*, **140**, 725-740, 1983.
- Scott, D. R., D. A. Lockner, J. D. Byerlee, and C. G. Sammis, Triaxial testing of Lopez fault gouge at 150 MPa mean effective stress, *Pure Appl. Geophys.*, **142**, 749-775, 1994.
- Shea, W. T., and A. K. Kronenberg, Strength and anisotropy of foliated rocks with varied mica contents, *J. Struct. Geol.*, **15**, 1097-1121, 1993.
- Sibson, R. H., Continental fault structure and the shallow earthquake source, *J. Geol. Soc. London*, **140**, 741-767, 1983.
- Sibson, R. H., Loading of faults to failure, *Bull. Seismol. Soc. Am.*, **81**, 2493-2497, 1991.
- Sleep, N. H., Ductile creep, compaction, and rate and state dependent friction within major fault zones, *J. Geophys. Res.*, this issue.
- Sleep, N. H., and M. L. Blanpied, Creep, compaction and the weak rheology of major faults, *Nature*, **359**, 687-692, 1992.
- Sleep, N. H., and M. L. Blanpied, Ductile creep and compaction: A mechanism for transiently increasing fluid pressure in mostly sealed fault zones, *Pure Appl. Geophys.*, **143**, 9-40, 1994.
- Stesky, R. M., W. F. Brace, D. K. Riley, and P.-Y. F. Robin, Friction in faulted rock at high temperature and pressure, *Tectonophysics*, **23**, 177-203, 1974.
- Stesky, R. M., The mechanical behavior of faulted rock at high temperature and pressure, Ph.D. thesis, 197 pp., Mass. Inst. of Technol., Cambridge, 1975.
- Stesky, R. M., Mechanisms of high temperature frictional sliding in Westerly granite, *Can. J. Earth Sci.*, **15**, 361-375, 1978a.
- Stesky, R. M., Rock friction—Effect of confining pressure, temperature and pore pressure, *Pure Appl. Geophys.*, **116**, 690-704, 1978b.
- Stuart, W. D., Forecast model for great earthquakes at the Nankai Trough subduction zone, *Pure Appl. Geophys.*, **126**, 619-641, 1988.
- Tchalenko, J. S., Similarities between shear zones of different magnitudes, *Geol. Soc. Am. Bull.*, **81**, 1625-1640, 1970.
- Tse, S. T., and J. R. Rice, Crustal earthquake instability in relation to the depth variation of frictional slip properties, *J. Geophys. Res.*, **91**, 9452-9472, 1986.
- Tullis, J., and R. A. Yund, Hydrolytic weakening of experimentally deformed Westerly granite and Hale albite rock, *J. Struct. Geol.*, **2**, 439-451, 1980.
- Tullis, T. E., Rock friction constitutive behavior from laboratory experiments and its implications for an earthquake prediction field monitoring program, *Pure Appl. Geophys.*, **126**, 555-588, 1988.
- Tullis, T. E., and J. D. Weeks, Constitutive behavior and stability of frictional sliding of granite, *Pure Appl. Geophys.*, **124**, 384-414, 1986.
- Weeks, J. D., N. M. Beeler, T. E. Tullis, L. A. Reinen and M. L. Blanpied, Velocity dependence of frictional behavior of simulated granite gouge to large displacement (abstract), *Eos Trans. AGU*, **71**, 1578, 1990.
- Wintsch, R. P., R. Christoffersen, and A. K. Kronenberg, Fluid-rock reaction-weakening of fault zones, *J. Geophys. Res.*, this issue.
- Yund, R. A., M. L. Blanpied, T. E. Tullis and J. D. Weeks, Observations of experimental fault gouges using transmission electron microscopy, *J. Geophys. Res.*, **95**, 15,589-15,602, 1990.

---

M. L. Blanpied, D. A. Lockner, and J. D. Byerlee, U.S. Geological Survey, 345 Middlefield Road, Mail Stop 977, Menlo Park, CA 94025. (email: mblanpied@isdmnl.wr.usgs.gov; dlockner@isdmnl.wr.usgs.gov; jbyerlee@isdmnl.wr.usgs.gov)

(Received March 14, 1994; revised March 6, 1995; accepted March 13, 1995.)